Genetic underpinnings of risky behaviour relate to altered neuroanatomy

Aydogan, Gökhan ; Daviet, Remi ; Karlsson Linnér, Richard ; Hare, Todd A ; Kable, Joseph W ; Kranzler, Henry R ; Wetherill, Reagan R ; Ruff, Christian C ; Koellinger, Philipp D ; Nave, Gideon

Abstract: Previous research points to the heritability of risk-taking behaviour. However, evidence on how genetic dispositions are translated into risky behaviour is scarce. Here, we report a genetically informed neuroimaging study of real-world risky behaviour across the domains of drinking, smoking, driving and sexual behaviour in a European sample from the UK Biobank (N = 12,675). We find negative associations between risky behaviour and grey-matter volume in distinct brain regions, including amygdala, ventral striatum, hypothalamus and dorsolateral prefrontal cortex (dlPFC). These effects are replicated in an independent sample recruited from the same population (N = 13,004). Polygenic risk scores for risky behaviour, derived from a genome-wide association study in an independent sample (N = 297,025), are inversely associated with grey-matter volume in dlPFC, putamen and hypothalamus. This relation mediates roughly 2.2% of the association between genes and behaviour. Our results highlight distinct heritable neuroanatomical features as manifestations of the genetic propensity for risk taking.

DOI: https://doi.org/10.1038/s41562-020-01027-y

1

Figure #	**Figure title** One sentence only	**Filename** This should be the name the file is saved as when it is uploaded to our system. Please include the file extension. i.e.: *Smith_ED Fig1.jpg*	**Figure Legend** If you are citing a reference for the first time in these legends, please include all new references in the Online Methods References section, and carry on the numbering from the main References section of the paper.
Extended Data Fig. 1	Bivariate correlations between variables used in the main study sample (N = 12,675).	Extended Data Figure 1.jpg	N/A
Extended Data Fig. 2	Empirical distributions of variables in the replication sample (N = 13,004).	Extended Data Figure 2.tiff	N/A
Extended Data Fig. 3	Effect sizes (standardized betas) of associations between risky behaviour and grey matter volume (GMV) in voxel clusters showing significant associations at P < .01% (FWE-corrected) (N = 12,675).	Extended Data Figure 3.jpg	Coordinates of peak association for each cluster are reported in parentheses (in mm). Standard errors denote uncorrected 95% confidence intervals. See Extended Data Table 4 for further details.
Extended Data Fig. 4	Effect sizes (standardized betas) of association between risky behaviour and IDPs of grey matter volume (GMV) showing significant associations	Extended Data Figure 4.jpg	Standard errors denote uncorrected 95% confidence intervals.

	at P<0.01 level (FWE-corrected) (N = 12,675).		
Extended Data Fig. 5	Associations (p-values) between risky behaviour and 148 ROI-level imaging-derived phenotypes (IDPs) of grey matter volume (GMV), controlling for cognitive and socioeconomic outcomes (N = 11,864).	Extended Data Figure 5.eps	Control variables include education years, fluid IQ, zip-code level social deprivation, household income, number of household members, birth location, and all standard controls.
Extended Data Fig. 6	Associations (p-values) between risky behaviour and 148 ROI-level imaging-derived phenotypes (IDPs) of grey matter volume (GMV), controlling for current drinking levels (binned in deciles) and smoking levels (binned in 3 categories) in addition to all standard controls (N = 12,675).	Extended Data Figure 6.eps	N/A
Extended Data Fig. 7	Meta-analysis of functional MRI studies of risky behaviours, provided by Neurosynth (N = 4,717 participants and K = 101 studies).	Extended Data Figure 7.jpg	Conjunction with areas showing negative GMV association with risky behaviour (including thalamus, vmPFC, amygdala and dlPFC) is marked in magenta (see Supplementary Table S1). Additional meta-analytic functional activation areas are marked in red.
Extended Data Fig. 8	Meditation analysis of	Extended Data Figure	The sum of all GMV differences in right dlPFC, putamen and hypothalamus

	the association between PRS and risky behaviour with GMV in dlPFC, putamen and hypothalamus (N = 12,675).	8.jpg	(based on the activation masks from Fig 5A) mediated ~2.07% of the association between the PRS and risky behaviour. Arrows depict the direction of the structural equation modelling and do not imply causality

2
3
4

5 **1. Supplementary Information:**

6

7 **A. Flat Files**

8

Item	**Present?**	**Filename** This should be the name the file is saved as when it is uploaded to our system, and should include the file extension. The extension must be .pdf	**A brief, numerical description of file contents.** i.e.: *Supplementary Discussion, Supplementary Figures 1-4, Supplementary Tables 1-4, Supplementary References.*
Supplementary Information	Yes	Supplementary_Information.pdf	Supplementary Methods, Supplementary Discussion, Supplementary Tables 1 - 9, Supplementary References, Supplementary Notes.
Reporting Summary	Yes	Reporting_Summary.pdf	
Peer Review Information	Yes	PRFile_Nave.pdf	

Genetic Underpinnings of Risky Behaviour Relate to Altered Neuroanatomy

Gökhan Aydogan[1], Remi Daviet[2], Richard Karlsson Linnér[3], Todd A. Hare[1], Joseph W. Kable[2,4], Henry R. Kranzler[5,6], Reagan R. Wetherill[5], Christian C. Ruff[1], Philipp D. Koellinger[3,7], BIG BEAR Consortium[8], Gideon Nave*[2]

[1]Zurich Center for Neuroeconomics (ZNE), Department of Economics, University of Zurich, Zurich, Switzerland

[2]Marketing Department, The Wharton School, University of Pennsylvania, Philadelphia, PA, USA

[3]Department of Economics, School of Business and Economics, Vrije Universiteit Amsterdam, Amsterdam, the Netherlands

[4]Department of Psychology, University of Pennsylvania, Philadelphia, PA, USA

[5]Department of Psychiatry, University of Pennsylvania Perelman School of Medicine, Philadelphia, PA, USA

[6]Veterans Integrated Service Network 4, Mental Illness Research, Education and Clinical Center, Crescenz Veterans Affairs Medical Center, Philadelphia, PA, USA

[7] La Follette School of Public Affairs, University of Wisconsin-Madison, Madison, WI, USA

[8] A list of authors and their affiliations appears at the end of the paper

[*]Corresponding author. gnave@wharton.upenn.edu

Abstract

Previous research points to the heritability of risk-taking behaviour. However, evidence on how genetic dispositions are translated into risky behaviour is scarce. Here, we report a genetically-informed neuroimaging study of real-world risky behaviour across the domains of drinking, smoking, driving, and sexual behaviour, in a European sample from the UK Biobank (*N*=12,675). We find negative associations between risky behaviour and grey matter volume (GMV) in distinct brain regions, including amygdala, ventral striatum, hypothalamus, and dorsolateral prefrontal cortex (dlPFC). These effects replicate in an independent sample recruited from the same population (*N*=13,004). Polygenic risk scores for risky behaviour, derived from a genome-wide association study in an independent sample (*N*=297,025), are inversely associated with GMV in dlPFC, putamen, and hypothalamus. This relation mediates ~2.2% of the association between genes and behaviour. Our results highlight distinct heritable neuroanatomical features as manifestations of the genetic propensity for risk taking.

Main

Taking risks—an essential element of many human experiences and achievements—requires balancing uncertain positive and negative outcomes. For instance, exploration, innovation and entrepreneurship can yield great benefits, but are also prone to failure[1]. Conversely, excessive risk-taking in markets can have enormous societal costs, such as the generation of speculative price bubbles[2]. Similarly, common behaviours such as *smoking, drinking, sexual promiscuity,* or *speeding* are considered rewarding by many but might expose individuals and those around them to deleterious health, social, and financial consequences. In 2010, the combined economic burden in the United States of these risky behaviours was estimated to be about $593.3 billion[3–6]. Although previous findings point to the partial heritability of risk tolerance and risky behaviours[7] and neuroanatomical measures exhibit high heritability[8,9], little is known about the brain features involved in translating genetic dispositions into risky behavioural phenotypes[8].

Recent research using structural brain-imaging data from small, non-representative samples (comprising up to a few hundred participants) has identified several neuroanatomical associations with risk tolerance[10–12]. However, this literature is limited by low statistical power[13,14], and the generalizability of their findings to other populations is questionable. Small sample sizes have also limited the ability to control systematically for many factors that could confound observed relations between brain features and risky behaviour, such as height[15] and genetic population structure[16,17]. Moreover, despite evidence that the effects of genetic factors are likely mediated by their influence on the brain and its development[7,18], neuroscientific and genetic approaches to understanding the biology of risky behaviour have largely proceeded in

isolation–perhaps due to the lack of large study samples that include both genetic and brain imaging measures.

Here, we utilize data obtained in a prospective epidemiological study of ~500,000 individuals aged 40 to 69 years [the UK Biobank (UKB)[19,20]] to carry out a pre-registered investigation (https://osf.io/qkp4g/, see Supplementary Methods for deviations from the analysis plan) of the relationship between individual differences in brain anatomy and the propensity to engage in risky behaviour across four domains (*N*=12,675, for sample characteristics see Figure 1 and Extended Data Figure 1). We replicate our findings in an independent sample recruited from the same population (*N*=13,004, for sample characteristics see Extended Data Figure 2). Further, we isolate specific differences in brain anatomy that are linked to the genetic disposition for risky behaviour— quantified via polygenic risk scores (PRS) derived from a genome-wide association study (GWAS) in an independent sample (*N* = 297,025)—and investigate how these neuroanatomical endophenotypes mediate the influence of genetics on the behavioural phenotype.

Results

Grey Matter Volume Associations with Risky Behaviour

Akin to a previous investigation[7], we construct a measure of risky behaviour by extracting the first principal component from four self-reported measures of drinking, smoking, speeding on motorways, and sexual promiscuity (*N* = 315,855; see Figure 2A, Supplementary Methods 1.1and Supplementary Tables 1-2 for descriptive statistics). This measure of risky behaviour is genetically correlated with many other traits, including cannabis use (r_g = 0.72, *SE* = 0.02), general risk tolerance (r_g = 0.56, *SE* = 0.02), self-employment (r_g = 0.52; *SE* = 0.30), suicide attempt (r_g = 0.47, *SE* = 0.07), antisocial behaviour (r_g = 0.45, *SE* = 0.14), extraversion (r_g = 0.34, *SE* = 0.04), and age

at first sexual experience (r_g = -0.54, *SE* = 0.02) (Supplementary Methods 1.5 and Supplementary Table 3). Thus, our measure is partly rooted in genetic differences between people and relates to a broad range of relevant events and behaviours.

Our main analysis includes a sample of 12,675 European-ancestry participants from the UKB. We first regress our measure of risky behaviour on total (whole-brain) grey matter volume (GMV) while controlling for age, birth year, gender, handedness, height, total intracranial volume and the first 40 genetic principal components, which account for genetic population structure (see Supplementary Methods 1.2). To exclude confounding effects of excessive alcohol consumption[21], we excluded from the analysis all current or former heavy drinkers (see Methods)[22,23]. We find an inverse association between total GMV and risky behaviour (standardized β = −.122; 95% confidence interval (CI) [−.156, −.087]; $t(12{,}561) = -6.92$; $P < 4.86 \times 10^{-12}$, two-sided).

To identify specific brain regions related to risky behaviour, we perform a whole-brain voxel-based morphometry (VBM)[24] analysis that regresses our measure of risky behaviour separately on GMV in each voxel across the brain, adjusting for the same control variables. We identify localized inverse associations between risky behaviour and GMV in distinct regions, only some of which were expected based on previous small-scale studies (see Figure 2B, Extended Data Figure 3 and Supplementary Table 4). In subcortical areas, we identify associations bilaterally in expected areas such as the amygdala and ventral striatum (VS), as well as in less expected areas such as the posterior hippocampus, putamen, thalamus, hypothalamus, and cerebellum. We also identify bilateral associations between risky behaviour and GMV in cortical regions that include the ventral medial prefrontal cortex (vmPFC), dorsolateral prefrontal cortex (dlPFC), ventro-anterior insula (aINS) and the precentral gyrus. In all of these regions,

GMV is negatively associated with the propensity to engage in risky behaviours. We find no positive associations between GMV and risky behaviour anywhere in the brain.

To quantify effect sizes of the associations between risky behaviour and GMV in anatomically-defined brain structures and to investigate the convergence of our findings across MRI processing pipelines[25], we conduct a follow-up analysis at the region of interest (ROI) level. This analysis primarily relies on the imaging-derived phenotypes (IDPs) provided by the UKB brain imaging processing pipeline[8,26,27], which used parcellations from the Harvard-Oxford cortical and subcortical atlases and the Diedrichsen cerebellar atlas. We derived additional IDPs using unbiased masks based on the results of the voxel-level analysis (see Supplementary Methods 1.3.3). This analysis identifies negative associations between risky behaviour and GMV in 23 anatomical structures, with standardized βs between −0.079 and −0.036 (see Figure 2C, Extended Data Figure 4 and Supplementary Table 5; for the associations between the IDPs and the individual measures that construct our phenotype of Risky Behavior, see Supplementary Table 6), the largest of which is in the right ventro-aINS; (β = −0.079; 95% CI [−.103, −.055]; $t(12{,}562) = -6.43$; $P_{uncorr} = 1.34 \times 10^{-10}$, two-sided).

We carry out several additional analyses to assess the differential contributions of various factors to the associations we observe. First, we re-estimate the ROI-level regressions with additional controls for various socioeconomic and cognitive outcomes that may be linked to both brain anatomy and risky behaviour, either as antecedents or downstream consequences. These controls include participants' years of education and fluid intelligence (13-item measure)[17], a zip-code level measure of the Townsend social deprivation index[28], household income and size, and birth location binned into 100 geographical clusters (see Supplementary Methods 1.2 and Figure 1). The direction and magnitude of all ROI effects are comparable to the main analysis (range of standardized

151 *βs* between −0.079 and −0.035), with the largest effect again located in the right ventro-
152 aINS (β = −0.079; 95% CI [−.104, −.055]; $t(11,647) = -6.29$; $P_{uncorr} = 3.3 \times 10^{-10}$, two-
153 sided). Furthermore, 19 of the 23 ROIs (all except the left Cuneal Cortex, left Crus I of
154 the Cerebellum, left Planum Polare and the Brain Stem) are statistically significant after
155 correction for multiple comparisons in this analysis (see Extended Data Figure 5 and
156 Supplementary Table 5).

157 Second, we re-estimate our ROI-level regressions with additional controls for
158 current levels of drinking (binned into 10 deciles) and smoking (binned into 3
159 categories). Although introducing these controls into the model regresses out variance
160 of interest from the main outcome measure, which likely attenuates the effects, this
161 analysis allows us to test whether any of the identified associations can reliably be
162 attributed to risky behaviour that is not limited to the substance-use domain. In this
163 analysis, we find that all of the effects originally identified remain negative in sign, yet
164 are smaller in magnitude (range of standardized βs between −0.041 and −0.011; see
165 Supplementary Table 7). Nonetheless, the effects in 9 subcortical ROIs (including the
166 Amygdala, Putamen, VS and Cerebellum) remain statistically significant after correction
167 for multiple comparisons (see Extended Data Figure 6), with the strongest association
168 identified in the left Amygdala (β = −0.041; 95% CI [-0.059, -0.023]; $t(12,551) = -4.4$;
169 $P_{uncorr} = 1.1 \times 10^{-5}$, two-sided). Thus, these subcortical IDPs are reliably associated with
170 risky behaviour in non-substance use domains.
171
172 **Replication in an Independent Sample**
173 Several months after the completion of our original analyses (in February 2020;
174 https://biobank.ndph.ox.ac.uk/showcase/exinfo.cgi?src=timelines), the UKB released
175 brain images of 20,316 additional participants— providing us with an opportunity to

replicate our findings in an independent dataset that contains the same variables, and participants recruited in the same way from the same population[29]. After applying the same exclusion criteria as in our original analysis, our replication sample consists of 13,004 participants, roughly the same size as our original sample (see Methods for details and Extended Figure 1 for sample characteristics). We repeat both the voxel-level and ROI-level analyses in this dataset. In the voxel-level analysis, we apply a significance threshold that corresponds to a family-wise-error (FWE) rate of 5% in all voxels that showed significance in the original analysis (p_{uncorr} = 2.956 x 10^{-04}, with t_{uncorr}(12,892) = 3.62, two-sided). We find that 92.6% of the original voxels (located in 20 of the 21 clusters originally identified, with the exception of a cluster in cerebellar lobules I-IV) successfully replicate (see Figure 3). Furthermore, the un-thresholded *t*-map[25] of the original dataset strongly correlates with the un-thresholded *t*-map of the replication dataset (r = .767; 95% CI [.766, .768]; $P < 10^{-10}$, two-sided). Likewise, our ROI-level analysis successfully replicates 21 of the original 23 ROI-level findings (p_{uncorr} = 3.35 x 10^{-03}, with t_{uncorr}(12,892) = 2.93, two-sided; see Supplementary Table 8). The two ROIs that do not replicate are the Cuneal Cortex (left) and the cerebellar lobule II (left).

Overlap between Grey Matter Volume Differences and Functional MRI (fMRI) Meta-Analysis

To investigate whether the neuroanatomical associations of real-world risky behaviour correspond spatially with the localized activation patterns commonly identified in fMRI studies of risky decision-making, we conduct a conjunction analysis to compare our VBM results with data obtained from a publicly available meta-analysis of fMRI studies of risky behaviour[30] (N = 4,717 participants, K = 101 individual studies, see Supplementary Table 9). The analysis reveals several brain regions whose anatomical

associations with risky behaviour converge with functional engagement, including the thalamus, amygdala, vmPFC, and dlPFC (see Figure 4 and Extended Data Figure 7).

Association of Polygenic Risk Scores for Risky Behaviour with Grey Matter Volume

Finally, we explore whether participants' genetic disposition for risky behaviour, proxied via their polygenic risk scores (PRS), are associated with the neuroanatomical correlates of the trait, and test whether these neuroanatomical correlates mediate the relationship between genetic predisposition and behaviour. To this end, we first conducted a GWAS in an independent sample of UKB participants of European ancestry (N=297,025), exclusive of 18,796 genotyped individuals with usable MRI images (main sample) and their relatives. From the GWAS, we constructed a PRS that aggregated the effects of 1,176,729 single nucleotide polymorphisms (SNPs) on risky behaviour for all of the participants with MRI data in our independent target sample (see Supplementary Methods 1.4). The PRS predicts ~3% of the variance in risky behaviour in our target sample. Although we find no statistically significant evidence to suggest that the PRS are associated with whole-brain GMV (standardized β = −.015; 95% CI [-.05 .02]; t(12,561) = −0.82; P > 0.41, two-sided), they are inversely associated with GMV in distinct regions, specifically the right dlPFC, right putamen and hypothalamus (Figure 5A.; regressions include all standard control variables, including total intracranial volume). Thus, GMV in these specific brain areas is negatively associated with the genetic disposition for risky behaviour.

Based on these results, we use the previously extracted GMV of these three ROIs to examine whether it mediates the observed gene-behaviour associations. A structural equation model including all standard controls reveals that ~2.2% of the

association between the PRS and risky behaviour is mediated through individual differences in GMV in the three regions (indirect path c'; standardized β = 0.004, 95%; CI [.002, .005]; z = 4.83; $P = 1.4 \times 10^{-06}$, two-sided) (see Figure 5B and Extended Data Figure 8).

Discussion

We investigate in a genetically-informed neuroimaging study (a) the association between GMV and real-world risky behaviour in a large population sample of European ancestry (main sample of 12,675 individuals and replication sample of 13,004 individuals), and (b) how the genetic disposition for risky behaviour is linked to GMV differences in a network of distinct brain areas. Several of the areas whose GMVs are linked to risky behaviour in this study have also often been functionally engaged during risky decision-making in small-scale fMRI studies that used stylized tasks. For instance, such correlations have been observed in the aINS, thalamus, dlPFC, vmPFC and VS[31,32]. These findings have led to proposals that upward and downward risks are encoded by distinct circuits, with upward risk mainly represented by areas encoding rewards (VS and vmPFC) and downward risk encoded by areas related to avoidance and negative arousal (aINS). Here, we substantiate previous functional studies with large-scale evidence that the structural properties of the same areas relate to risky behaviour in an ecologically valid setting[33] when long-term health consequences are at stake.

Our results extend previous findings by showing that the neural foundation of risky behaviour is complex. Our analyses identify additional negative associations between risky behaviour and GMV in several areas, including the cerebellum, posterior hippocampus, hypothalamus, and putamen. While it is not yet clear how structural differences are manifested in properties of brain function[34], our results suggest that risk

taking draws on manifold neural processes, not just the representation and integration of upward and downward risks in the brain. Specifically, considering previous meta-analyses, the areas identified in this study are involved broadly in memory (posterior hippocampus), emotion processing (amygdala, ventro-aINS)[35], neuroendocrine processes (hypothalamus)[36,37], reward processing (vmPFC, VS and putamen)[38] and executive functions (dlPFC)[39]. Thus, it appears that risky behaviour taps into multiple elements of human cognition, ranging from inhibitory control[40] to emotion regulation[41] and the integration of outcomes and risks[42]. This mirrors previous findings showing that risky behaviour is also a genetically complex trait[7].

Additionally, our results underscore the long-suspected role of the hypothalamic–pituitary–adrenal (HPA) axis in regulating risk-related behaviours, in line with hormonal studies that link risky behaviour and sensation seeking to stress responsivity[36,37,43–45]. Furthermore, our finding that risky behaviour is linked to the structure of several cerebellar areas confirms the under-appreciated importance of the cerebellum for human cognition and decision-making, and highlights the need for further research on the specific behavioural contributions of this brain area[46].

Of note, it remains an open question the extent to which the differences in GMV that we identify can be ascribed to specific heritable micro-anatomical traits, such as neuronal size, dendritic or axonal arborisation, or relative count of different cell types[47]. Moreover, it is not yet clear how these individual differences, in turn, influence behaviour. Nonetheless, our results provide evidence that neuro-anatomical structure constitutes the micro-foundation for neuro-computational mechanisms underlying individual differences in risky behaviours[34].

Several of the observed neuroanatomical correlates of risky behaviour are also associated with the genetic disposition for the phenotype. Specifically, we find that GMV

in the hypothalamus, the putamen and the dlPFC share variance with both risky behaviour and its polygenic risk score. This finding extends previous studies showing correlational[36,42,43] and causal evidence[37,48] of the involvement of these areas in risky behaviour by indicating that a genetic component partly underlies the associations. Although our analyses cannot identify the direction of the causal relationships (see Supplementary Discussion for an additional discussion of limitations), they show that risky behaviour and its genetic associations share variance with distinct GMV features and provide an overarching framework for how the genetic dispositions for risky behaviour may be expressed in the corresponding behavioural phenotype.

Our results are also in line with the bioinformatic annotation of the largest GWAS on risk tolerance to date, conducted in over 1 million individuals[7], which implicated specific areas in the prefrontal cortex (BA9, BA24), striatum, cerebellum and the amygdala. However, bioinformatics tools used for GWAS annotation cannot be considered conclusive, as they rely on gene expression patterns in relatively small samples of (post-mortem) human brains or non-human samples[49]. Moreover, they cannot speak to whether changes in a particular tissue or cell type have negative or positive effects on the phenotype or how strong the effects are. Here, we show an alternative approach to annotating GWAS findings using a different type of data (large-scale population samples that include *in-vivo* brain scans and genetic data), relying on different assumptions than those used by bioinformatics tools. Our results add new insight by showing that lower GMV in specific brain areas is related to more risky behaviour and by implicating brain regions (i.e., putamen, hypothalamus, and dlPFC) in addition to those previously annotated. The effect sizes we observe here (standardized $\beta < 0.08$) are an order of magnitude larger than those found in GWAS on risky behaviour, but they nonetheless require very large samples for detection.

Finally, while many features of the brain are heritable, the environment indisputably plays an important role in brain development. We therefore see our results not as independent from, or of greater importance than, the effects of environmental and developmental factors. Rather, our study constitutes one step towards understanding how the complex development of human risky behaviour may be constrained by genetic factors.

Methods

Sample Characteristics and Selection Criteria

Main sample. We use publicly available data from the UKB, which recruited 502,617 people aged 40 to 69 years from the general population across the United Kingdom[19,20]. All UKB participants provided written informed consent and the study was granted ethical approval by the North West Multi-Centre Ethics committee. Our initial sample consists of 18,796 individuals with brain scans and genotype data, all of the imaged UKB participants as of October 2018. We excluded participants with putative sex chromosome aneuploidy (N = 6) or a mismatch between genetic and reported sex (N = 10), participants of non-European ancestry (N = 893), and participants who did not pass the UKB quality-control thresholds (N = 14), described in Bycroft et al.[27]. To minimize the potential influence of neurotoxic effects due to excessive alcohol intake[21,22], we also excluded current heavy drinkers (531 females consuming more than 18 drinks per week and 793 males consuming more than 24 drinks per week)[22,23]. To exclude potential former drinkers, we also removed 426 participants who indicated that they did not drink alcohol.

All structural T1 MRI images used in the study underwent automated quality control by the UKB brain imaging processing pipeline[26]. We performed two additional

quality checks using the Computational Anatomy Toolbox (CAT; www.neuro.uni-jena.de/cat/) for SPM 12 (www.fil.ion.ucl.ac.uk/spm/software/spm12/). First, we relied on the CAT12 automated Image and Pre-processing quality assessment, which included quality parameters for resolution, noise, and bias of images, 57 of which were automatically excluded and not pre-processed due to low image quality. Second, after pre-processing, we utilized an automated quality check of sample homogeneity to identify outliers that exhibited substantially different GMV patterns than the rest of the sample (see the CAT12 manual for details; http://www.neuro.uni-jena.de/cat12/CAT12-Manual.pdf, p. 17ff). In total, we excluded 690 individuals with scans of high image inhomogeneity (two standard deviations below the mean). Finally, we excluded 2,701 participants with incomplete behavioural data of interest or control variables. Our final dataset consists of N = 12,675 individuals.

Replication sample. The initial replication sample consisted of 20,316 individuals with usable brain scans and genotype data, all of the imaged UKB participants as of February 2020 who were not included in our main sample. Following the original analysis, we excluded participants with putative sex chromosome aneuploidy (N = 7), a mismatch between genetic and reported sex (N = 11), non-European ancestry (N = 1,143), heavy drinking or abstinence from alcohol (N = 1,376), and those that did not pass the UKB quality-control thresholds (N = 31)[27]. All T1 MRI images used in the study underwent the same quality control procedure as in our original sample, resulting in the removal of additional 391 individuals. Finally, we excluded participants with incomplete data (N = 4,353). Our final replication sample consists of N = 13,004. The empirical distributions of the variables characterizing our replication analysis are depicted in Extended Data Figure 2.

Measures

Risky Behaviour. We closely follow Karlsson Linnér et al.[7] to derive a measure of risky behaviour across domains based on participants' self-reports of: (1) Number of alcoholic drinks per week, (2) Ever having smoked, (3) Number of sexual partners, and (4) Frequency of driving faster than the motorway speed limit (see Supplementary Methods 1.1). We perform principal component analysis (PCA) on N = 315,855 UKB participants and extract the first principal component (PC) of the four measures as the main outcome of interest (referred to as "risky behaviour"). The first PC explains ~37% of the variance in the four measures, and it is the only PC that loads positively on all of them. Summary statistics and factor loadings of the PCA are available in Supplementary Tables 1 and 2. The code for generating the variable of 'risky behaviour' is accessible at https://osf.io/qkp4g/.

Control variables. The full list of control variables and the methods used to generate them are available in Supplementary Methods 1.2.

T1 MRI Image Processing. We use T1-weighted structural brain MRI images in NIFTI format provided by the UKB. Images were acquired using 3-T Siemens Skyra scanners, with a 32-channel head coil (Siemens, Erlangen, Germany), with the following scanning parameters: repetition time = 2000 ms; echo time = 2.1 ms; flip angle = 8°; matrix size = 256 × 256 mm; voxel size = 1 × 1 × 1 mm; number of slices = 208. A detailed description of the methods used to pre-process the images and derive voxel-level and ROI-level IDPs is available in Supplementary Methods 1.3.1-1.3.3.

Polygenic Risk Score (PRS) for Risky Behaviour. To construct a PRS, we first re-estimated the GWAS of our main measure described in ref[7] after excluding 18,796 genotyped individuals with usable T1 MRI images and their relatives up to the third degree (final GWAS sample: *N* = 297,025 individuals of European ancestry). The GWAS was performed using linear mixed models (LMM), implemented via BOLT-LMM

version 2.3.2[50]. Next, we performed quality control (QC) of the GWAS results using a standardized QC protocol, described in detail in ref[7]. This protocol removes rare and low-quality single-nucleotide polymorphisms (SNPs) based on minor allele frequency (MAF) < 0.001, imputation quality (INFO) < 0.7, and SNPs that could not be aligned with the Haplotype Reference Consortium (HRC) reference panel, among other filters. After QC, a total of 11,514,220 SNPs remained in the GWAS summary statistics. Thereafter, we calculated a PRS for each participant by weighting their genotype across SNPs by the corresponding regression coefficients estimated in the GWAS (see Supplementary Methods 1.4 for further information).

Analysis

Voxel-based Morphometry (VBM). We identify associations between risky behaviour and localized GMV across the brain using whole-brain voxel-based morphometry (VBM), a method that normalizes the anatomical brain images of all participants in one stereotactic space[24]. We regress risky behaviour separately on each voxel of the smoothed GMV images (see Supplementary Methods 1.3.1) and the control variables. We correct for multiple comparisons by adjusting the FWE rate to α = 0.01 using permutation tests (p_{uncorr} = 1.248 x 10^{-06}, with $|t_{uncorr}|$ = 4.85, two-sided). See Extended Data Figure 3 and Supplementary Table 4 for the summary statistics of each cluster and the coordinates of the peak voxel within that cluster.

Region of Interest (ROI)-level Analysis. We compute the associations between risky behaviour and 139 IDPs of GMV extracted by the UKB brain imaging processing pipeline[26] using parcellations from the Harvard-Oxford cortical and subcortical atlases and Diedrichsen cerebellar atlas, in addition to 9 IDPs derived using unbiased masks based on the results of our voxel-level analysis (see Supplementary Methods 1.3.2 and 1.3.3). We regress risky behaviour separately on each IDP and the control variables

401 and correct for multiple comparisons by adjusting the FWE rate of α = 0.01 using
402 permutation tests (p_{uncorr} = 9.37 x 10^{-05}, with $|t_{uncorr}|$= 3.91, two-sided).
403 **Replication of the Voxel-level and ROI-level Analyses.** We repeat the VBM analyses
404 in the replication sample for all voxels that showed significance in the original sample,
405 correcting for multiple comparisons by adjusting the FWE rate to α = 0.05 (two-tailed)
406 using permutation tests (p_{uncorr} = 2.956 x 10^{-04}, with t_{uncorr} = 3.62). We also repeat the
407 ROI-level analysis in all ROIs that showed significance in the original sample, and
408 correct for multiple comparisons by adjusting the FWE rate to α = 0.05 (two-tailed) using
409 permutation tests (p_{uncorr} = 3.35 x 10^{-03}, with t_{uncorr} = 2.93). We define replication success
410 as observing a statistically significant effect at the 5% level (corrected for multiple
411 hypothesis testing) in the same direction as the original finding[51].
412 **Comparison of VBM Results with a Meta-Analysis of Functional MRI (fMRI)**
413 **Studies.** We compare our VBM results with a publicly available meta-analysis of fMRI
414 studies provided by Neurosynth[30], an online platform for large-scale, automated
415 synthesis of fMRI data (https://neurosynth.org/). The meta-analysis was based on the
416 keyword 'risky'. It consisted of K = 101 individual studies with a total of N = 4,717
417 participants (see Supplementary Table 9 for details), and was conducted using a
418 uniformity test (assuming that random activations are evenly distributed across all
419 voxels). The meta-analytic statistical image was corrected for multiple comparisons by
420 applying a false discovery rate (FDR) of .01 (implemented by Neurosynth). The
421 summary of studies included in the meta-analysis is available on Supplementary Table
422 9. The 3D activation map that resulted from the meta-analysis is available on
423 https://neurosynth.org/analyses/terms/risky/. To compare our VBM results (i.e., brain
424 structure) with the meta-analysis of data on brain function, we perform a whole-brain
425 voxel-level conjunction analysis of the two (see Extended Data Figure 7) that exhibits

the spatial overlap of all voxels that are significant in both analyses (Figure 4). Thus, both the structure and function of the brain regions identified by this conjunction are significantly associated with risky behaviour.

Voxel-based Morphometry (VBM) Analysis of Risky Behaviour PRS. We repeat the VBM analysis in all voxels identified to be associated with risky behaviour, using the PRS as the dependent variable. This approach allows the identification of brain regions that were likely to mediate the effect of genetic disposition on risky behaviour. The PRS was constructed using GWAS results from an independent sample, to ensure that the effect size estimates in this analysis are not inflated due to overfitting. We account for multiple comparisons using a permutation test with an FWE rate of $p_{FWE} < 0.05$. This part of the analysis was not pre-registered.

Mediation Analysis. We conduct mediation analyses (implemented in STATA 14) to test whether GMV differences in the brain regions whose GMVs are associated with the PRS of risky behaviour (right dlPFC, right putamen and hypothalamus) mediate the association between the PRS and risky behaviour. We first extract GMV from these three ROIs using the same unbiased masks as in the ROI-level analysis (see Supplementary Methods 1.3.3). Then, we estimate a structural equation model (SEM) to quantify the effect of the PRS on risky behaviour mediated via GMV differences in these ROIs. All SEM equations include the aforementioned standard control variables (listed in Supplementary Methods 1.2). We carry out an additional robustness check by estimating an SEM that assumes one single path (i.e., the sum of all ROIs), which yields the same pattern of results (see Extended Data Figure 8).

Family-Wise-Error Correction using Permutation Tests. To account for multiple hypothesis testing, we determine the appropriate FWE corrected *p*-value threshold with a permutation test procedure in each of our analyses[52]. To this end, we generated

1,000 datasets with randomly permuted phenotypes (i.e., breaking the link between the outcome and explanatory variables), estimated regression models for all IDPs per analysis, and recorded the lowest *p*-value of each run to generate an empirical distribution of the test statistic under the null hypothesis. To obtain the FWE rate of any given alpha, we use the n^{th} = α x 1000 lowest *p*-value from the 1,000 permutation runs as the FWE corrected *p*-value threshold.

Pre-registration of Analysis Plan and Unplanned Deviations. We pre-registered our analysis plan on Open Science Framework (OSF, https://osf.io/qkp4g/, registered Dec. 2018). Our pre-registered plan specified the construction of the dependent variable, the control variables, the inclusion criteria and quality controls, the VBM analyses and the main ROI-level analyses. We summarize all deviations from the analysis plan in Supplementary Methods 2.

Data Availability

Data and materials are available via UK Biobank at http://www.ukbiobank.ac.uk/.

Code Availability

The analysis code used in this study is publicly available on https://osf.io/qkp4g/.

BIG BEAR Consortium

Gökhan Aydogan[1], Remi Daviet[2], Richard Karlsson Linnér[3], Todd A. Hare[1], Joseph W. Kable[2,4], Henry R. Kranzler[5,6], Reagan R. Wetherill[5], Christian C. Ruff[1], Philipp D. Koellinger[3,7], Gideon Nave[2]

[1] Zurich Center for Neuroeconomics (ZNE), Department of Economics, University of Zurich, Zurich, Switzerland

[2] Marketing Department, The Wharton School, University of Pennsylvania, Philadelphia, PA, USA

[3] Department of Economics, School of Business and Economics, Vrije Universiteit Amsterdam, Amsterdam, the Netherlands

[4] Department of Psychology, University of Pennsylvania, Philadelphia, PA, USA

[5] Department of Psychiatry, University of Pennsylvania Perelman School of Medicine, Philadelphia, PA, USA

[6] Veterans Integrated Service Network 4, Mental Illness Research, Education and Clinical Center, Crescenz Veterans Affairs Medical Center, Philadelphia, PA, USA

[7] La Follette School of Public Affairs, University of Wisconsin-Madison, Madison, WI, USA

A full list of members and their affiliations appears in the Supplementary Information.

References

1. Knight, F. H. *Risk, Uncertainty, and Profit* (Houghton Mifflin, 1921).
2. Eckel, C. C. & Füllbrunn, S. C. Thar SHE Blows? Gender, Competition, and Bubbles in Experimental Asset Markets. *American Economic Review* **105(2),** 906–920 (2015).
3. Centers for Disease Control and Prevention. *Incidence, Prevalence, and Cost of Sexually Transmitted Infections in the United States*. https://www.cdc.gov/std/stats/sti-estimates-fact-sheet-feb-2013.pdf (2013).
4. Sacks, J. J., Gonzales, K. R., Bouchery, E. E., Tomedi, L. E. & Brewer, R. D. 2010 National and State Costs of Excessive Alcohol Consumption. *Am. J. Prev. Med.* **49(5),** e73–e79 (2015).
5. Blincoe, L., Miller, T. R., Zaloshnja, E. & Lawrence, B. A. *The economic and societal impact of motor vehicle crashes, 2010 (Revised)*. https://trid.trb.org/view/1311862 (2015).
6. U.S. Department of Health and Human Services. The Health Consequences of Smoking: 50 Years of Progress. A Report of the Surgeon General. *Atlanta, GA: U.S. Department of Health and Human Services, Centers for Disease Control and Prevention, National Center for Chronic Disease Prevention and Health Promotion, Office on Smoking and Health* (2014).
7. Linner, R. K. et al. Genome-wide association analyses of risk tolerance and risky behaviors in over 1 million individuals identify hundreds of loci and shared genetic influences. *Nat. Genet.* **51,** 245–257 (2019).
8. Elliott, L. T. et al. Genome-wide association studies of brain imaging phenotypes in UK Biobank. *Nature* **562,** 210–216 (2018).
9. Thompson, P. M. et al. Genetic influences on brain structure. *Nat. Neurosci.* **4,**

513 1253–1258 (2001).
514 10. Grubb, M. A., Tymula, A., Gilaie-Dotan, S., Glimcher, P. W. & Levy, I.
515 Neuroanatomy accounts for age-related changes in risk preferences. *Nat. Commun.*
516 **7,** 13822 (2016).
517 11. Jung, W. H., Lee, S., Lerman, C. & Kable, J. W. Amygdala Functional and
518 Structural Connectivity Predicts Individual Risk Tolerance. *Neuron* **98(2),** 394–
519 404.e4 (2018).
520 12. Nasiriavanaki, Z. et al. Prediction of individual differences in risky behavior in young
521 adults via variations in local brain structure. *Front. Neurosci.* **9,** 359 (2015).
522 13. Button, K. S. et al. Power failure: why small sample size undermines the reliability of
523 neuroscience. *Nat. Rev. Neurosci.* **14,** 365–376 (2013).
524 14. Marek, S. et al. Towards Reproducible Brain-Wide Association Studies. Preprint at
525 https://www.biorxiv.org/content/10.1101/2020.08.21.257758v1 (2020).
526 15. Dohmen, T. et al. INDIVIDUAL RISK ATTITUDES: MEASUREMENT,
527 DETERMINANTS, AND BEHAVIORAL CONSEQUENCES. *Journal of the*
528 *European Economic Association* **9(3),** 522–550 (2011).
529 16. Cardon, L. R. & Palmer, L. J. Population stratification and spurious allelic
530 association. *Lancet* **361(9357),** 598–604 (2003).
531 17. Nave, G., Jung, W. H., Linnér, R. K., Kable, J. W. & Koellinger, P. D. Are Bigger
532 Brains Smarter? Evidence From a Large-Scale Preregistered Study. *Psychol. Sci.*
533 **30(1),** 43-54 (2019).
534 18. Romer, D. Adolescent risk taking, impulsivity, and brain development: implications
535 for prevention. *Dev. Psychobiol.* **52(3),** 263–276 (2010).
536 19. Miller, K. L. et al. Multimodal population brain imaging in the UK Biobank
537 prospective epidemiological study. *Nature Neuroscience* **19,** 1523–1536 (2016).

20. Sudlow, C. et al. UK biobank: an open access resource for identifying the causes of a wide range of complex diseases of middle and old age. *PLOS Med.* **12(3),** e1001779 (2015).
21. Harper, C. The neurotoxicity of alcohol. *Hum. Exp. Toxicol.* **26(3),** 251–257 (2007).
22. Daviet, R. et al. Multimodal brain imaging study of 19,825 participants reveals adverse effects of moderate drinking. Preprint at https://www.biorxiv.org/content/10.1101/2020.03.27.011791v1 (2020).
23. Kranzler, H. R. et al. Topiramate Treatment for Heavy Drinkers: Moderation by a GRIK1Polymorphism. *American Journal of Psychiatry* **171(4),** 445–452 (2014).
24. Ashburner, J. & Friston, K. J. Voxel-Based Morphometry—The Methods. *Neuroimage* **11(6),** 805–821 (2000).
25. Botvinik-Nezer, R. et al. Variability in the analysis of a single neuroimaging dataset by many teams. *Nature* **582,** 84-88 (2020).
26. Alfaro-Almagro, F. et al. Image processing and Quality Control for the first 10,000 brain imaging datasets from UK Biobank. *Neuroimage* **166,** 400–424 (2018).
27. Bycroft, C. et al. The UK Biobank resource with deep phenotyping and genomic data. *Nature* **562,** 203–209 (2018).
28. Hill, W. D. et al. Molecular Genetic Contributions to Social Deprivation and Household Income in UK Biobank. *Curr. Biol.* **26(22),** 3083–3089 (2016).
29. Masouleh, S. K., Eickhoff, S. B., Hoffstaedter, F., Genon, S. & Alzheimer's Disease Neuroimaging Initiative. Empirical examination of the replicability of associations between brain structure and psychological variables. *eLife* **8,** e43464 (2019).
30. Yarkoni, T., Poldrack, R. A., Nichols, T. E., Van Essen, D. C. & Wager, T. D. Large-scale automated synthesis of human functional neuroimaging data. *Nat. Methods* **8,** 665–670 (2011).

31. Mohr, P. N. C., Biele, G. & Heekeren, H. R. Neural processing of risk. *J. Neurosci.* **30(19),** 6613–6619 (2010).
32. Wu, C. C., Sacchet, M. D. & Knutson, B. Toward an affective neuroscience account of financial risk taking. *Front. Neurosci.* **6,** 159 (2012).
33. Schonberg, T., Fox, C. R. & Poldrack, R. A. Mind the gap: bridging economic and naturalistic risk-taking with cognitive neuroscience. *Trends Cogn. Sci.* **15(1),** 11–19 (2011).
34. Kable, J. W. & Levy, I. Neural markers of individual differences in decision-making. *Curr. Opin. Behav. Sci.* **5,** 100–107 (2015).
35. Chang, L. J., Yarkoni, T., Khaw, M. W. & Sanfey, A. G. Decoding the role of the insula in human cognition: functional parcellation and large-scale reverse inference. *Cereb. Cortex* **23(3),** 739–749 (2013).
36. Evans, B. E., Greaves-Lord, K., Euser, A. S., Franken, I. H. A. & Huizink, A. C. The relation between hypothalamic-pituitary-adrenal (HPA) axis activity and age of onset of alcohol use. *Addiction* **107(2),** 312–322 (2012).
37. Kreek, M. J., Nielsen, D. A., Butelman, E. R. & LaForge, K. S. Genetic influences on impulsivity, risk taking, stress responsivity and vulnerability to drug abuse and addiction. *Nat. Neurosci.* **8(11),** 1450–1457 (2005).
38. O'Doherty, J. et al. Dissociable roles of ventral and dorsal striatum in instrumental conditioning. *Science* **304(5669),** 452–454 (2004).
39. Dosenbach, N. U. F., Fair, D. A., Cohen, A. L., Schlaggar, B. L. & Petersen, S. E. A dual-networks architecture of top-down control. *Trends Cogn. Sci.* **12(3),** 99–105 (2008).
40. Ivanov, I., Schulz, K. P., London, E. D. & Newcorn, J. H. Inhibitory control deficits in childhood and risk for substance use disorders: a review. *Am. J. Drug Alcohol*

588 *Abuse* **34(3),** 239–258 (2008). (Comma after volume number should be bold. Issue
589 number is missing.)
590 41. Heilman, R. M., Crişan, L. G., Houser, D., Miclea, M. & Miu, A. C. Emotion
591 regulation and decision making under risk and uncertainty. *Emotion* **10(2),** 257–265
592 (2010).
593 42. Tobler, P. N., Christopoulos, G. I., O'Doherty, J. P., Dolan, R. J. & Schultz, W. Risk-
594 dependent reward value signal in human prefrontal cortex. *Proc. Natl. Acad. Sci. U.*
595 *S. A.* **106(17),** 7185–7190 (2009).
596 43. Huizink, A. C., Ferdinand, R. F., Ormel, J. & Verhulst, F. C. Hypothalamic-pituitary-
597 adrenal axis activity and early onset of cannabis use. *Addiction* **101(11),** 1581–1588
598 (2006).
599 44. Margittai, Z. *et al.* Combined Effects of Glucocorticoid and Noradrenergic Activity on
600 Loss Aversion. *Neuropsychopharmacology* **43,** 334–341 (2018).
601 45. Grotzinger, A. D. et al. Hair and salivary testosterone, hair cortisol, and
602 externalizing behaviors in adolescents. *Psychol. Sci.* **29(5),** 688–699 (2018).
603 46. Buckner, R. L. The cerebellum and cognitive function: 25 years of insight from
604 anatomy and neuroimaging. *Neuron* **80(3),** 807–815 (2013).
605 47. Mechelli, A., Price, C. J., Friston, K. J. & Ashburner, J. Voxel-Based Morphometry
606 of the Human Brain: Methods and Applications. *Current Medical Imaging Reviews*
607 **1(2),** 105–113 (2005).
608 48. Knoch, D. et al. Disruption of right prefrontal cortex by low-frequency repetitive
609 transcranial magnetic stimulation induces risk-taking behavior. *J. Neurosci.* **26(24),**
610 6469–6472 (2006).
611 49. Allen Institute for Brain Science. BrainSpan atlas of the developing human brain.
612 http://www.brainspan.org/ (2015).

50. Loh, P. et al. Efficient Bayesian mixed-model analysis increases association power in large cohorts. *Nat. Genet.* **47,** 284–290 (2015).
51. Camerer, C. F. et al. Evaluating the replicability of social science experiments in *Nature* and *Science* between 2010 and 2015. *Nat. Hum. Behav* **2,** 637–644 (2018).
52. Dickie, D. A. et al. Permutation and parametric tests for effect sizes in voxel-based morphometry of gray matter volume in brain structural MRI. *Magnetic Resonance Imaging* **33(10),** 1299–1305 (2015).

Acknowledgments

This research was carried out under the auspices of the Brain Imaging and Genetics in Behavioural Research (https://big-bear-research.org/) consortium. The authors thank Nadja C. Furtner for helpful comments and Dylan Manfredi for research assistance. The research was conducted using UK Biobank resources under application 40830. The study was supported by funding from an NSF Early Career Development Program grant (1942917) and The Wharton School Dean's Research fund to G.N., an ERC Consolidator Grant to P.D.K. (647648 EdGe), and a Swiss National Science Foundation grant to C.C.R (100019L_173248). R.R.W. was financially supported by NIAAA K23 grant (K23 AA023894) and H.R.K. was supported by NIDA grant P30 DA046345. G.N. thanks Carlos and Rosa de la Cruz for ongoing support. The work was carried out on the Dutch national e-infrastructure with the support of the SURF Cooperative. The funders had no role in study design, data collection and analysis, decision to publish or preparation of the manuscript. Data can be accessed via the UKBiobank, and data analysis scripts are available on OSF (https://osf.io/qkp4g/).

Author contributions

G.A., R.D., J.W.K., P.D.K. and G.N. designed the research plan. G.N., P.D.K. and C.C.R. oversaw the study. G.A., R.D. and R.K.L analysed the data with critical input from P.D.K., G.N. and C.C.R.. G.A. G.N. and P.D.K. wrote the paper and Supplementary Materials. T.A.H, H.R.K and R.R.W. contributed to and critically reviewed the manuscript.

Competing interests

Dr. Kranzler is a member of an advisory board for Dicerna Pharmaceuticals; a member of the American Society of Clinical Psychopharmacology's Alcohol Clinical Trials

Initiative, which was sponsored in the past three years by AbbVie, Alkermes, Amygdala Neurosciences, Arbor Pharmaceuticals, Ethypharm, Indivior, Lilly, Lundbeck, Otsuka, and Pfizer; and is named as an inventor on PCT patent application #15/878,640 entitled: "Genotype-guided dosing of opioid agonists," filed January 24, 2018. All other authors declare no competing interests.

Figure Legends

Figure 1. | Main Sample Characteristics (*N*=12,675). (A) Geographical birth location clusters of the study's participants. Each star represents the birthplace of a participant (non-jittered). Colours denote 100 geographical clusters, calculated using a *k*-means clustering algorithm with *k* = 100 and 10,000 iterations after random seeding. (B) Empirical distributions of variables in the main study sample.

Figure 2. | Association between Risky Behaviour and Imaging-Derived Phenotypes (IDPs) of Grey Matter Volume (GMV). (A) Loadings for the first principal component are extracted from four self-reported measures of risky behaviour in the *drinking*, *smoking*, *driving* and *sexual* domains (*N* = 315,855) (see Figure 1 for descriptive statistics). We use this first principal component as a measure of risky behaviour. (B) Voxel-level GMV negatively associated with risky behaviour (*N* = 12,675). We observe associations in subcortical areas, including *thalamus*, *posterior hippocampus*, *amygdala*, *putamen, ventral striatum* and *cerebellum*. Associations with cortical areas include *posterior middle temporal gyrus*, *precentral gyrus*, *dlPFC*, *anterior insula* and *vmPFC*. (C) Associations between risky behaviour and GMV in 148 regions of interest (ROIs)` (*N* = 12,675). The grey dotted line shows the FWE corrected threshold of *P* = 0.01 (see Methods for details).

Figure 3 | Voxel-level Grey Matter Volumes (GMV) associated with risky behaviour in the replication sample (N = 13,004). 92.6% of the voxels identified

673 in our original analysis (located in 20 out of 21 original clusters identified,
674 marked in purple) successfully replicate (corrected for multiple testing at the 5%
675 level using a permutation test). Non replicated voxels are located in the
676 cerebellar lobules I-IV (marked in blue).

677

678

679 **Figure 4 |** Conjunction between the Grey Matter Volume (GMV) differences
680 associated with risky behaviour identified in the current study and the results of a
681 meta-analysis of 101 fMRI studies, based on the keyword “risky”. This analysis
682 identifies overlapping voxels in the thalamus, amygdala, vmPFC and dlPFC (see
683 Methods for details).

684

685

686 **Figure 5.** | Association of Polygenic Risk Scores (PRS) for Risky Behaviour and
687 Grey Matter Volume (GMV). (A) We constructed a PRS of risky behaviour from a
688 GWAS in an independent sample (*N*=297,025) and investigated its associations with
689 GMV in brain voxels that we identified as linked to risky behaviour. The PRS
690 negatively correlates with GMV in the right dlPFC, putamen and hypothalamus. **(B)**
691 GMV differences in hypothalamus (path 1, designated as a_1 and b_1), right putamen
692 (path 2, designated as a_2 and b_2) and right dlPFC (path 3, designated as a_3 and b_3)
693 mediate ~2.2% of the association between the PRS and risky behaviour. Arrows
694 depict the direction of the structural equation modelling and do not imply causality (*N*
695 = 12,675).

a

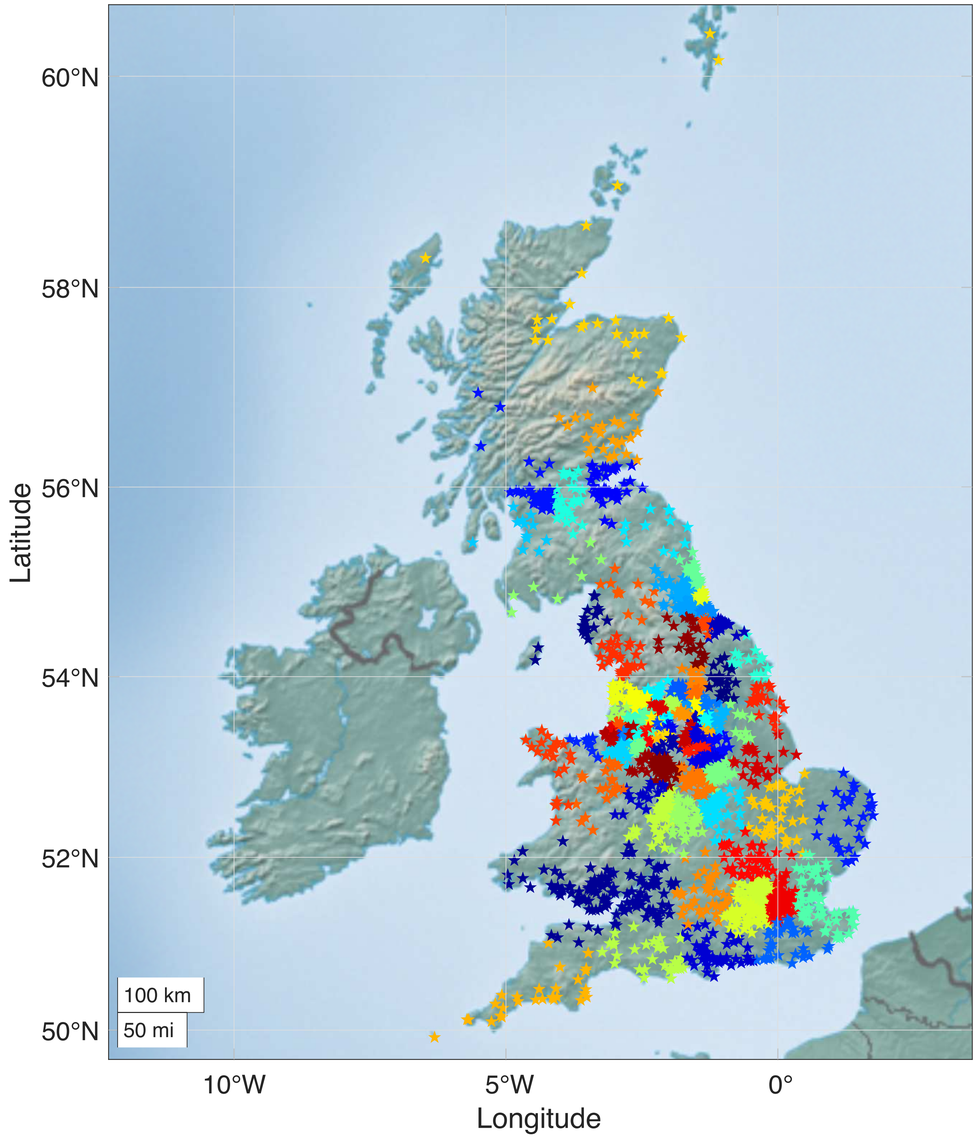
60°N
58°N
56°N
54°N
52°N
50°N
Latitude
10°W
5°W
0°
Longitude
100 km
50 mi

b

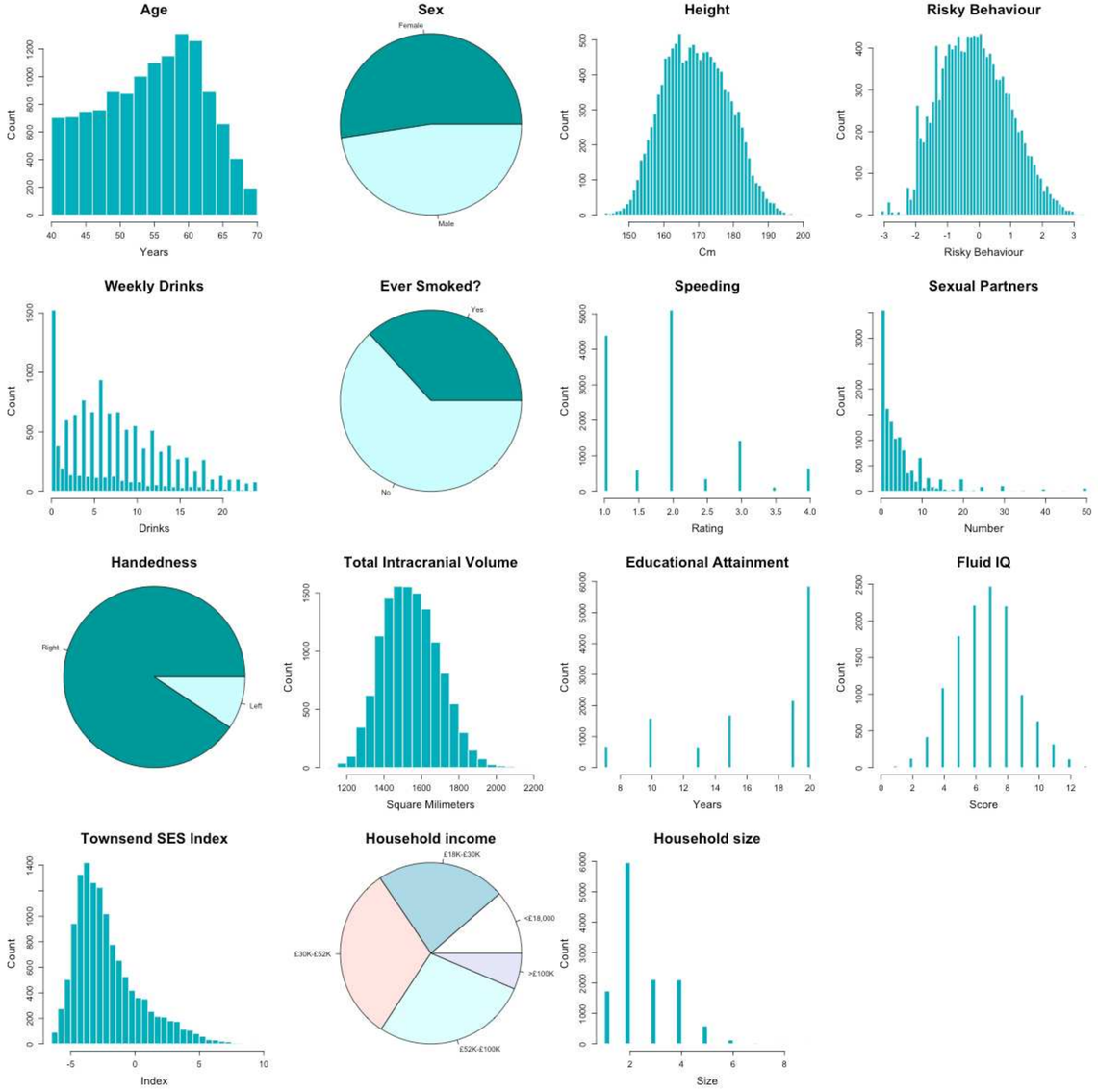
Age
Years
Count
Sex
Female
Male
Height
Cm
Risky Behaviour
Weekly Drinks
Drinks
Ever Smoked?
Yes
No
Speeding
Rating
Sexual Partners
Number
Handedness
Right
Left
Total Intracranial Volume
Square Milimeters
Educational Attainment
Years
Fluid IQ
Score
Townsend SES Index
Index
Household income
£18K-£30K
<£18,000
£30K-£52K
>£100K
£52K-£100K
Household size
Size

a

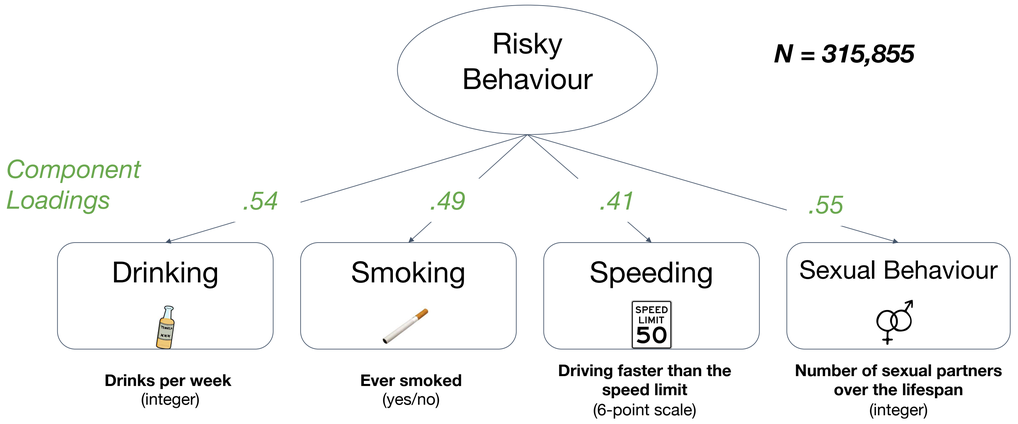
Risky Behaviour
N = 315,855
Component Loadings
.54
.49
.41
.55
Drinking
Smoking
Speeding
Sexual Behaviour
SPEED LIMIT 50
Drinks per week (integer)
Ever smoked (yes/no)
Driving faster than the speed limit (6-point scale)
Number of sexual partners over the lifespan (integer)

b

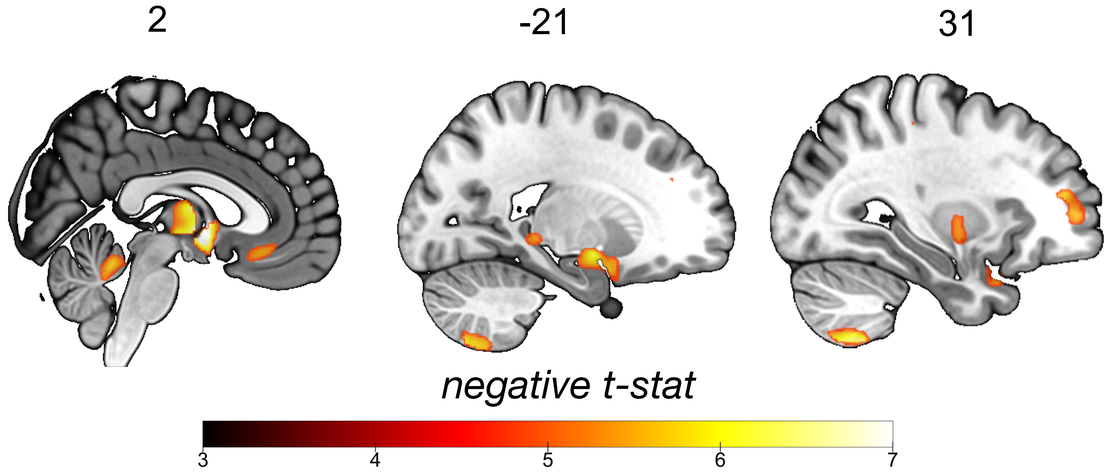
2
-21
31
negative t-stat
3
4
5
6
7

c

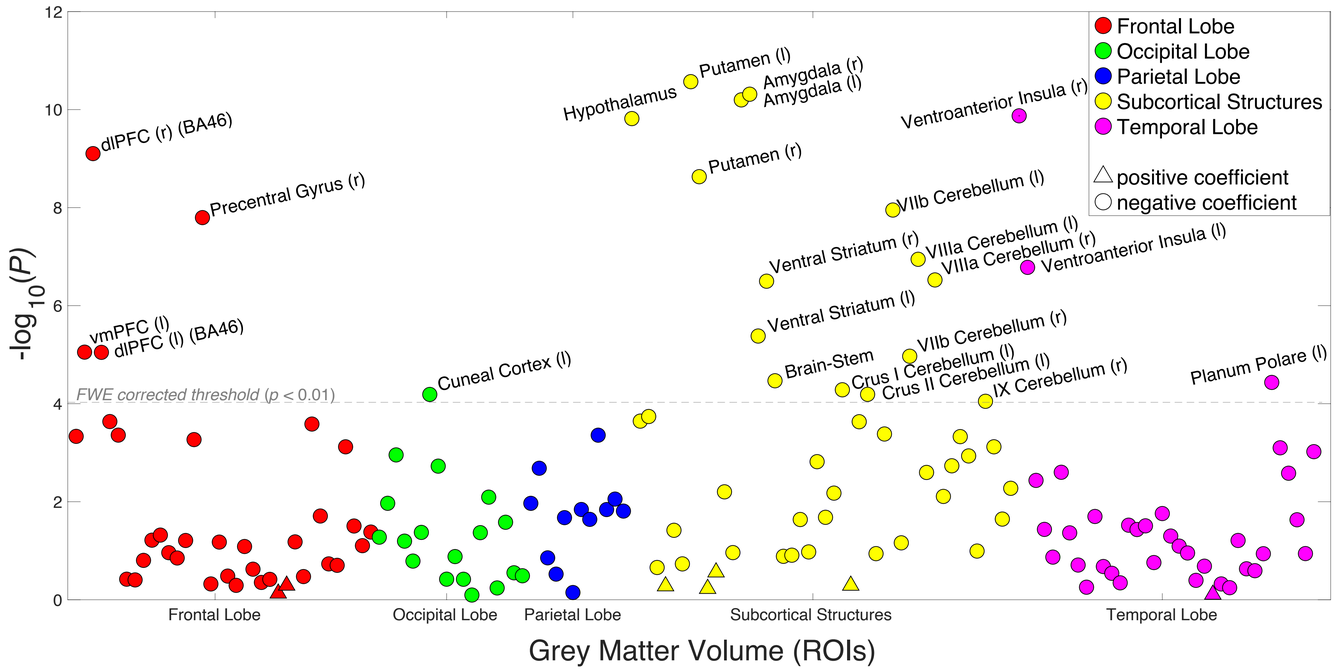
Frontal Lobe
Occipital Lobe
Parietal Lobe
Subcortical Structures
Temporal Lobe
positive coefficient
negative coefficient
dlPFC (r) (BA46)
Precentral Gyrus (r)
vmPFC (l)
dlPFC (l) (BA46)
Cuneal Cortex (l)
Hypothalamus
Putamen (l)
Amygdala (r)
Amygdala (l)
Putamen (r)
Ventroanterior Insula (r)
VIIb Cerebellum (l)
Ventral Striatum (r)
VIIIa Cerebellum (l)
VIIIa Cerebellum (r)
Ventroanterior Insula (l)
Ventral Striatum (l)
Brain-Stem
VIIb Cerebellum (r)
Crus I Cerebellum (l)
Crus II Cerebellum (l)
IX Cerebellum (r)
Planum Polare (l)
FWE corrected threshold (p < 0.01)
-log10(P)
Frontal Lobe
Occipital Lobe
Parietal Lobe
Subcortical Structures
Temporal Lobe
Grey Matter Volume (ROIs)

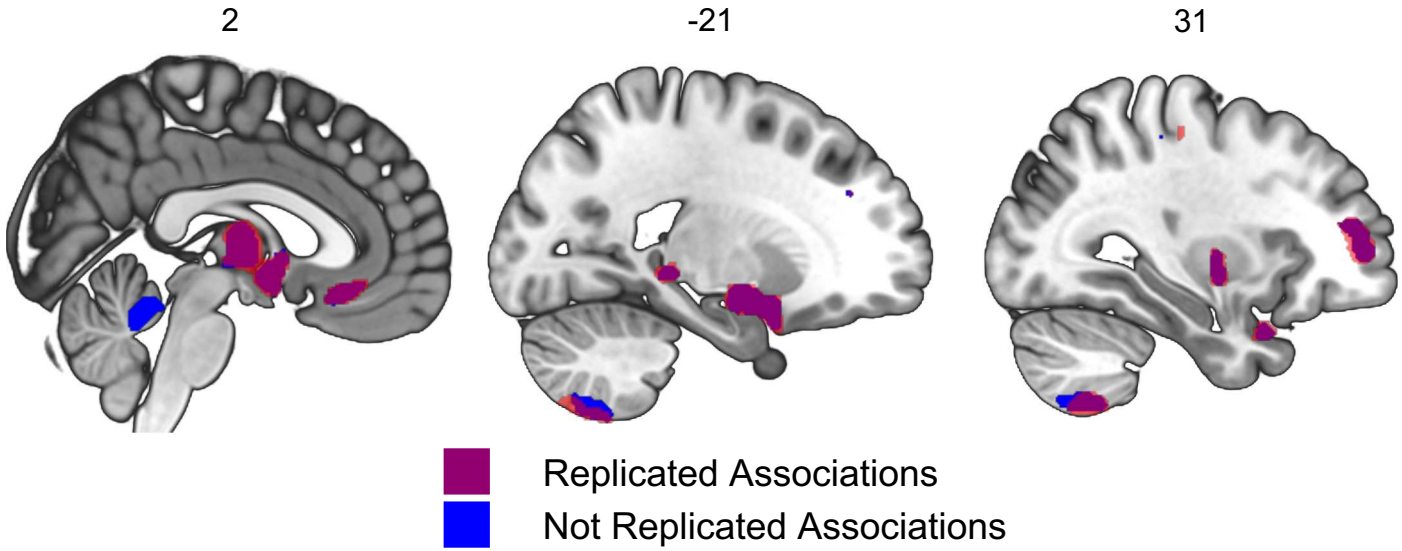
2
-21
31
Replicated Associations
Not Replicated Associations

2

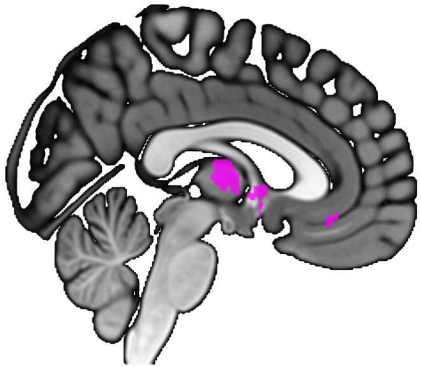

-21

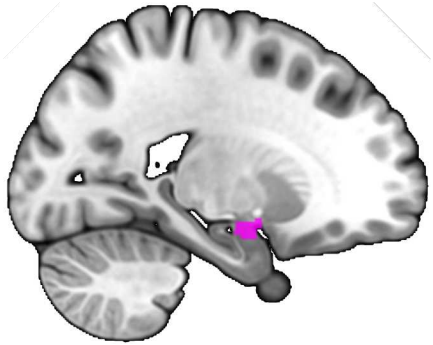

31

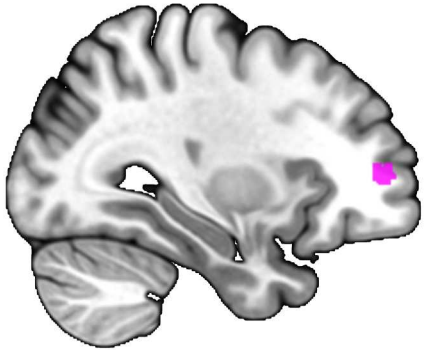

a

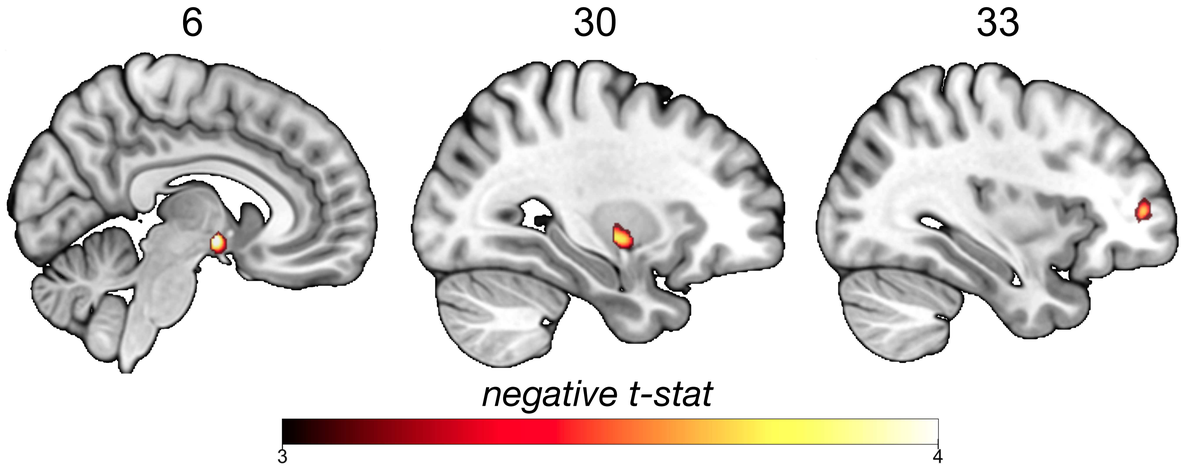
6
30
33
negative t-stat
3
4

b

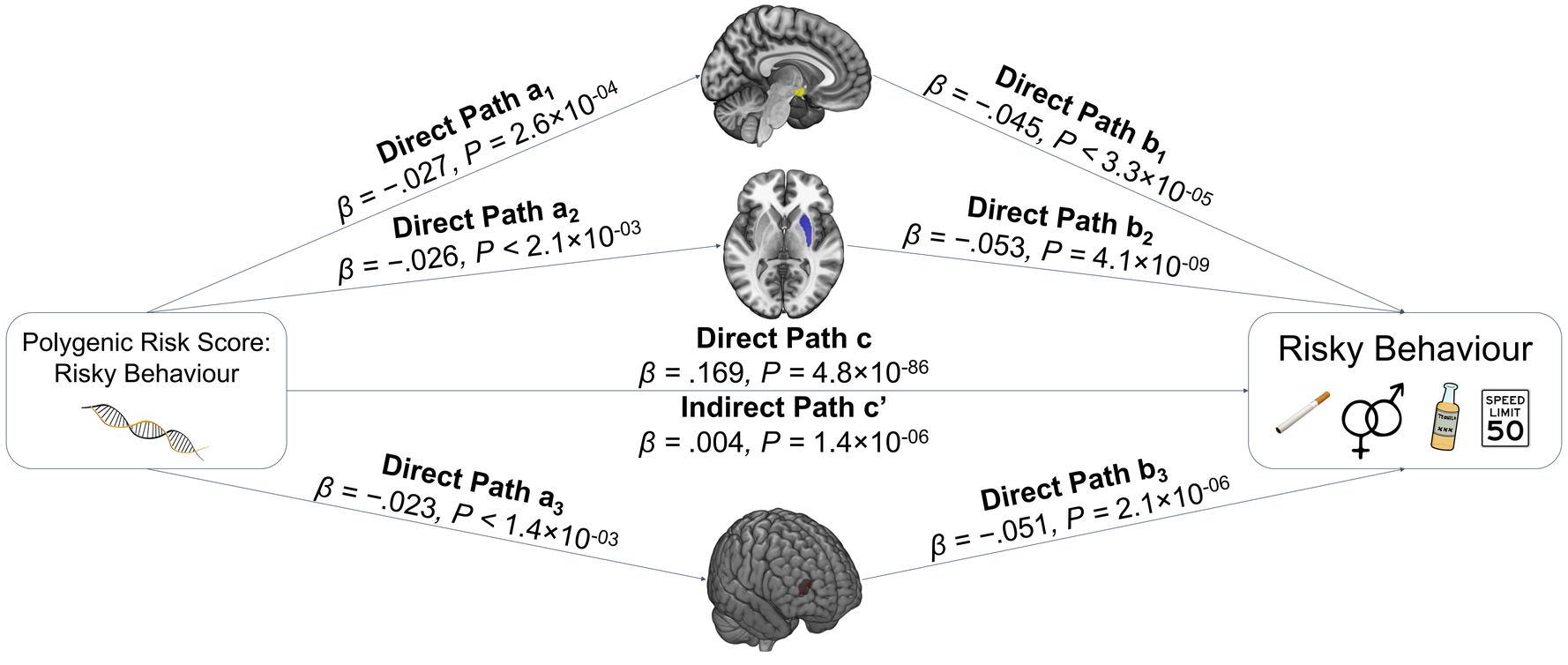
Direct Path a1
β = −.027, P = 2.6×10-04
Direct Path a2
β = −.026, P < 2.1×10-03
Direct Path b1
β = −.045, P < 3.3×10-05
Direct Path b2
β = −.053, P = 4.1×10-09
Polygenic Risk Score:
Risky Behaviour
Direct Path c
β = .169, P = 4.8×10-86
Indirect Path c'
β = .004, P = 1.4×10-06
Risky Behaviour
Direct Path a3
β = −.023, P < 1.4×10-03
Direct Path b3
β = −.051, P = 2.1×10-06
SPEED LIMIT 50

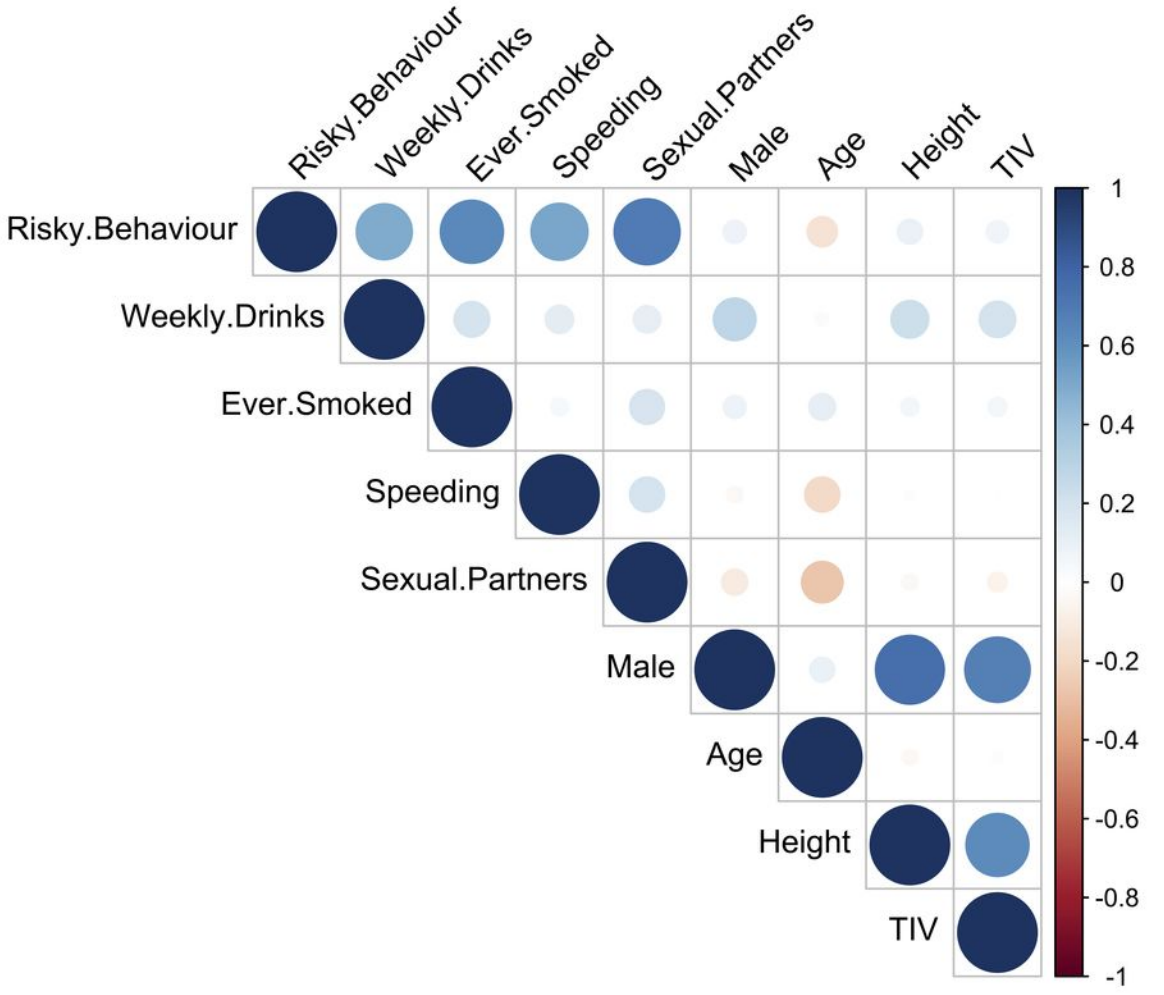
Risky.Behaviour
Weekly.Drinks
Ever.Smoked
Speeding
Sexual.Partners
Male
Age
Height
TIV
1
0.8
0.6
0.4
0.2
0
-0.2
-0.4
-0.6
-0.8
-1

Age

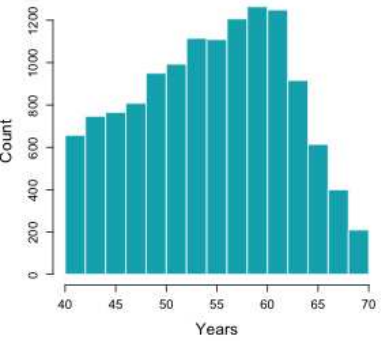

Sex

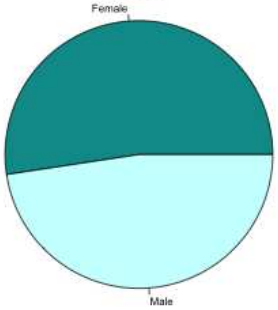

Height

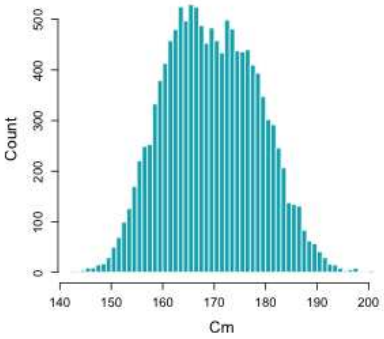

Risky Behaviour

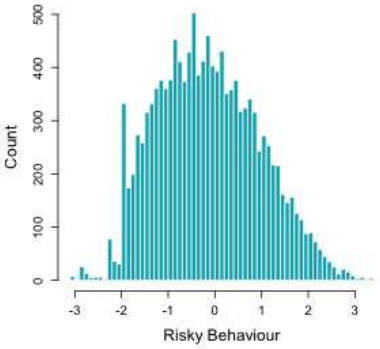

Weekly Drinks

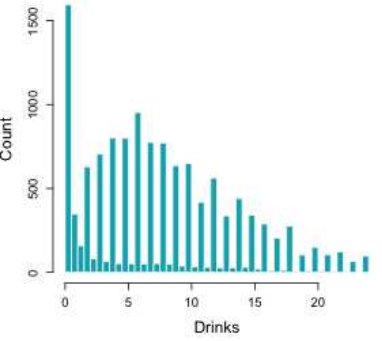

Ever Smoked?

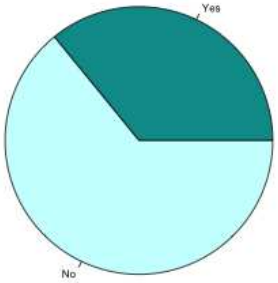

Speeding

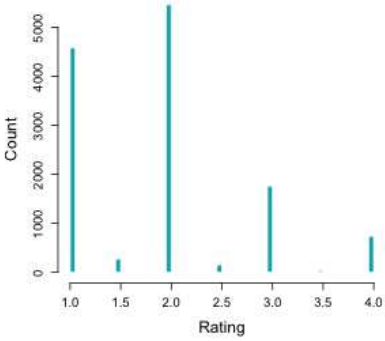

Sexual Partners

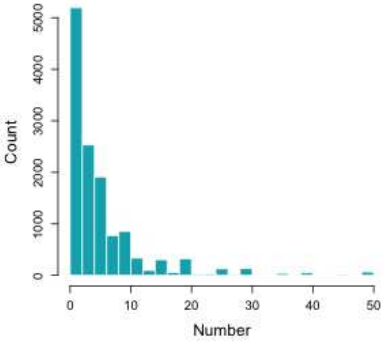

Handedness

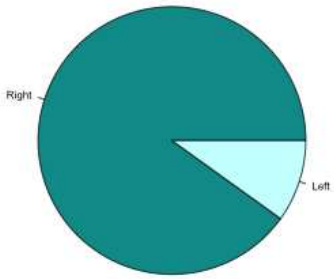

Total Intracranial Volume

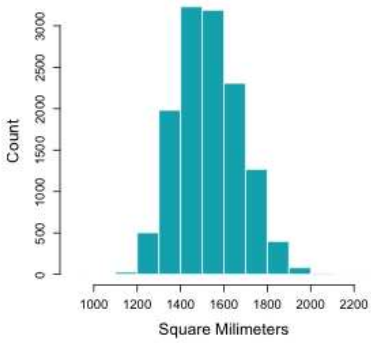

Educational Attainment

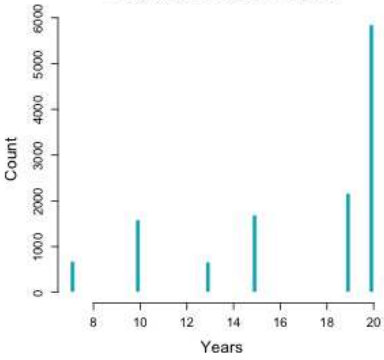

Fluid IQ

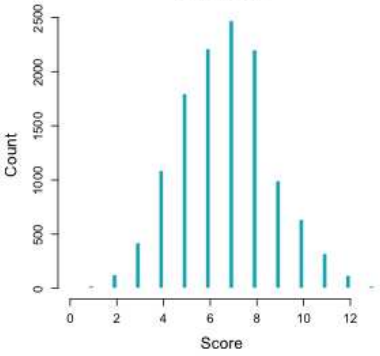

Townsend SES Index

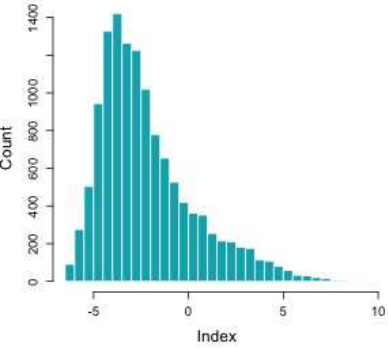

Household income

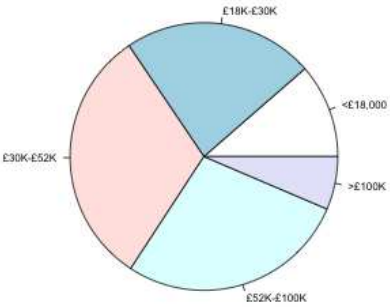

Household size

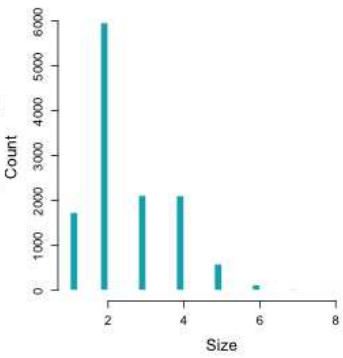

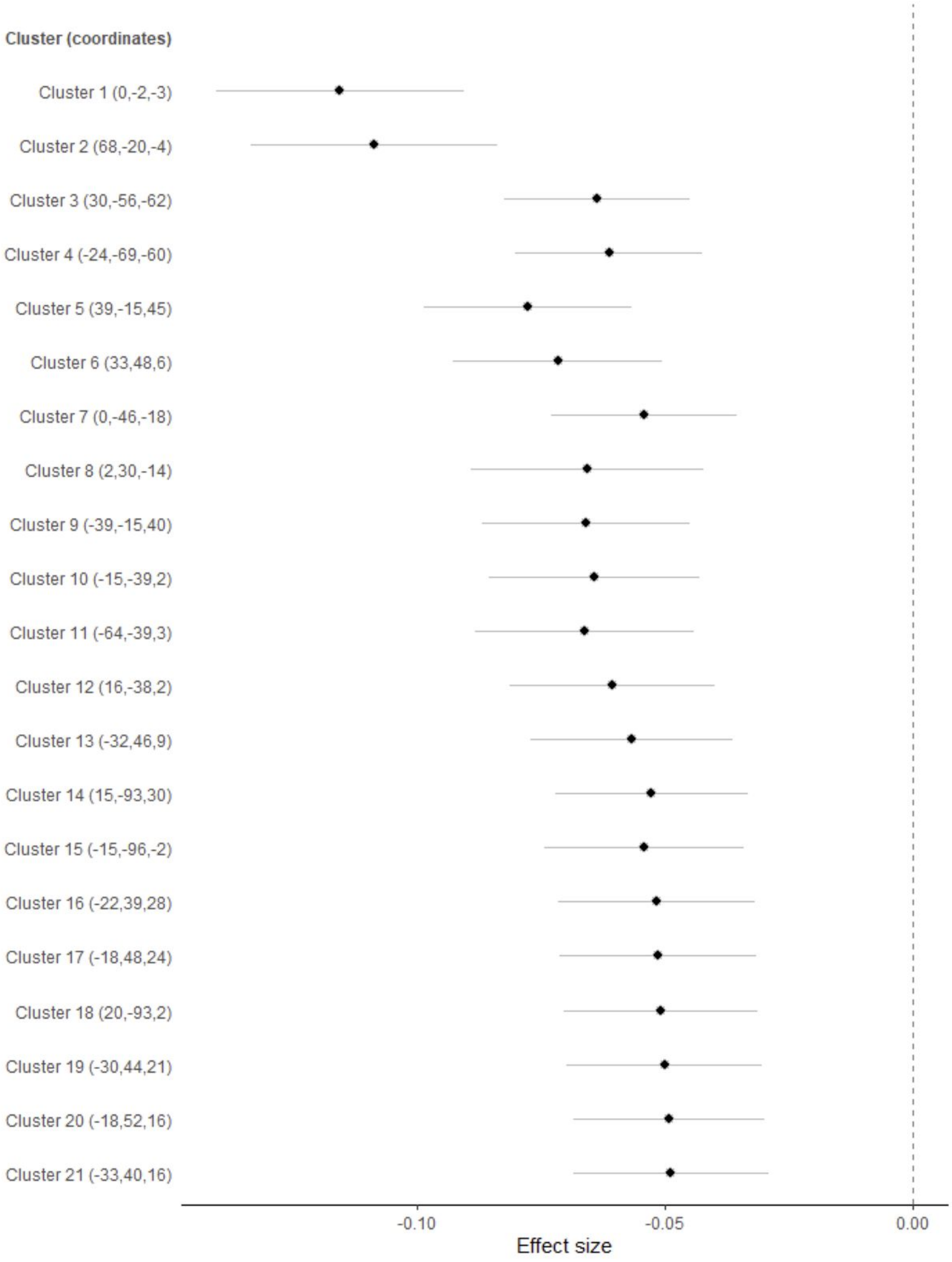
Cluster (coordinates)
Cluster 1 (0,-2,-3)
Cluster 2 (68,-20,-4)
Cluster 3 (30,-56,-62)
Cluster 4 (-24,-69,-60)
Cluster 5 (39,-15,45)
Cluster 6 (33,48,6)
Cluster 7 (0,-46,-18)
Cluster 8 (2,30,-14)
Cluster 9 (-39,-15,40)
Cluster 10 (-15,-39,2)
Cluster 11 (-64,-39,3)
Cluster 12 (16,-38,2)
Cluster 13 (-32,46,9)
Cluster 14 (15,-93,30)
Cluster 15 (-15,-96,-2)
Cluster 16 (-22,39,28)
Cluster 17 (-18,48,24)
Cluster 18 (20,-93,2)
Cluster 19 (-30,44,21)
Cluster 20 (-18,52,16)
Cluster 21 (-33,40,16)
-0.10
-0.05
0.00
Effect size

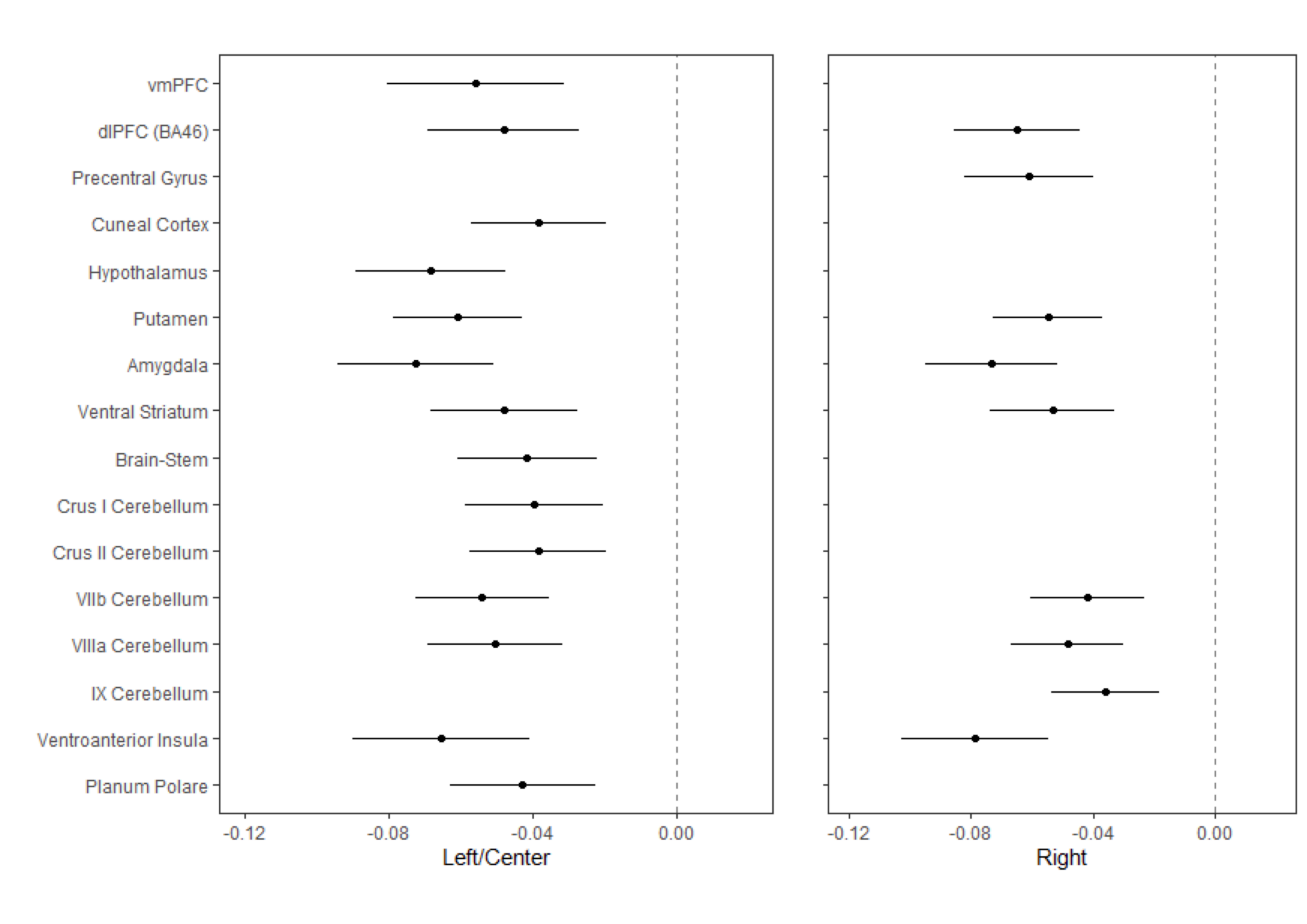
vmPFC
dlPFC (BA46)
Precentral Gyrus
Cuneal Cortex
Hypothalamus
Putamen
Amygdala
Ventral Striatum
Brain-Stem
Crus I Cerebellum
Crus II Cerebellum
VIIb Cerebellum
VIIIa Cerebellum
IX Cerebellum
Ventroanterior Insula
Planum Polare
-0.12
-0.08
-0.04
0.00
Left/Center
-0.12
-0.08
-0.04
0.00
Right

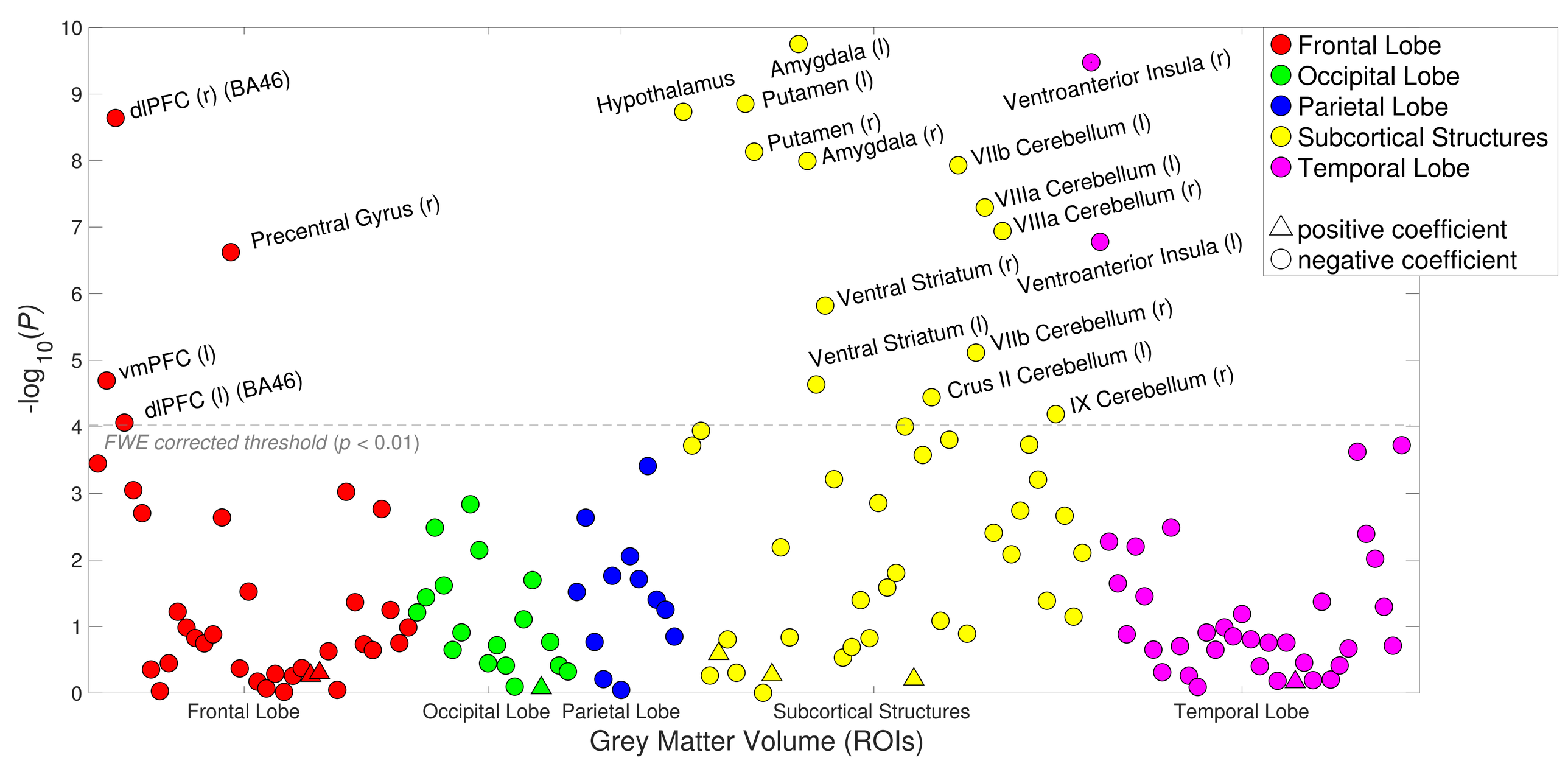
Frontal Lobe
Occipital Lobe
Parietal Lobe
Subcortical Structures
Temporal Lobe
positive coefficient
negative coefficient
dlPFC (r) (BA46)
Precentral Gyrus (r)
vmPFC (l)
dlPFC (l) (BA46)
Hypothalamus
Amygdala (l)
Putamen (l)
Putamen (r)
Amygdala (r)
Ventroanterior Insula (r)
VIIb Cerebellum (l)
VIIIa Cerebellum (l)
VIIIa Cerebellum (r)
Ventral Striatum (r)
Ventroanterior Insula (l)
Ventral Striatum (l)
VIIb Cerebellum (r)
Crus II Cerebellum (l)
IX Cerebellum (r)
FWE corrected threshold (p < 0.01)
-log10(P)
Frontal Lobe
Occipital Lobe
Parietal Lobe
Subcortical Structures
Temporal Lobe
Grey Matter Volume (ROIs)

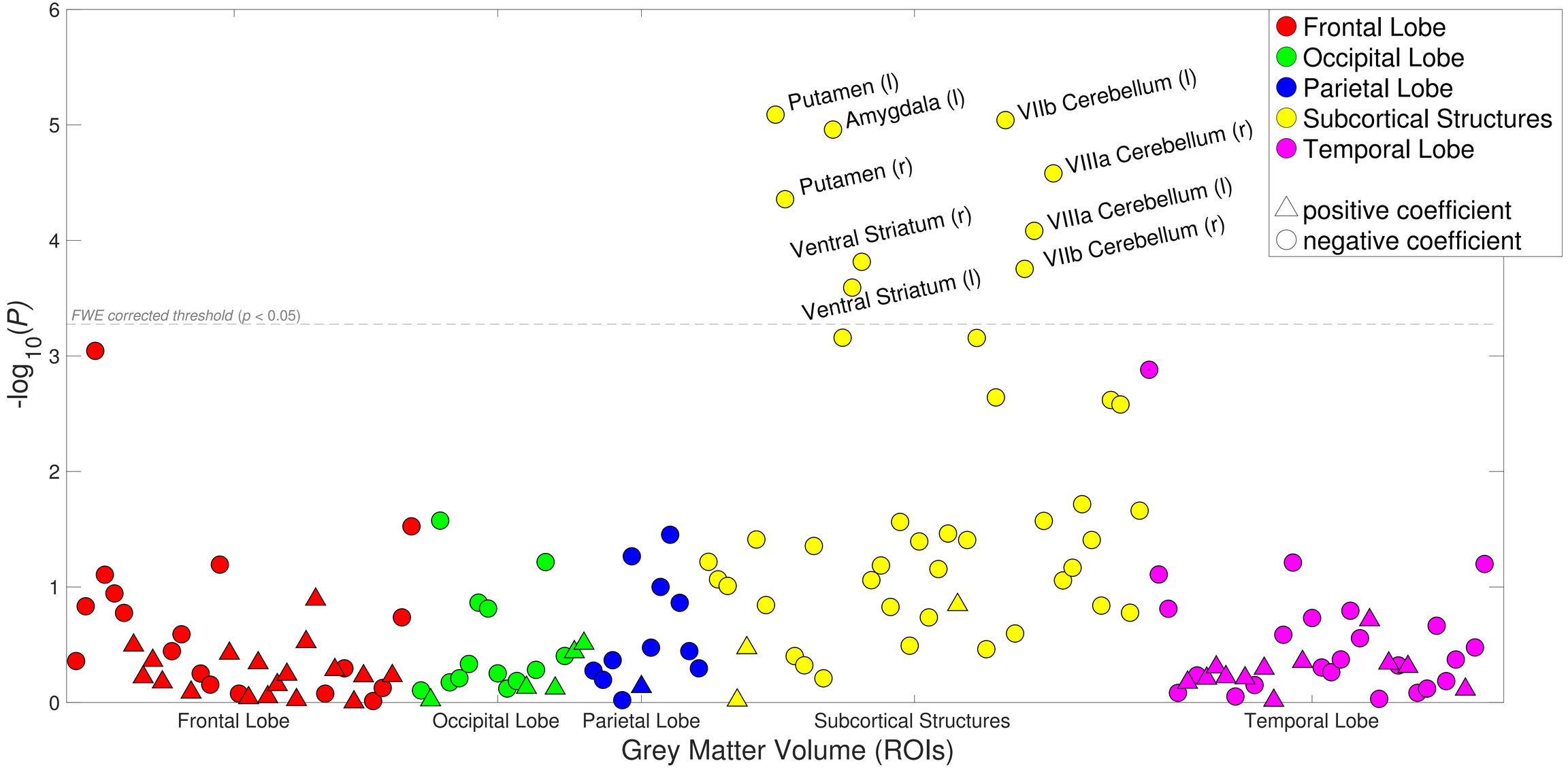
Frontal Lobe
Occipital Lobe
Parietal Lobe
Subcortical Structures
Temporal Lobe
positive coefficient
negative coefficient
Putamen (l)
Amygdala (l)
VIIb Cerebellum (l)
Putamen (r)
VIIIa Cerebellum (r)
Ventral Striatum (r)
VIIIa Cerebellum (l)
Ventral Striatum (l)
VIIb Cerebellum (r)
FWE corrected threshold (p < 0.05)
-log10(P)
0
1
2
3
4
5
6
Frontal Lobe
Occipital Lobe
Parietal Lobe
Subcortical Structures
Temporal Lobe
Grey Matter Volume (ROIs)

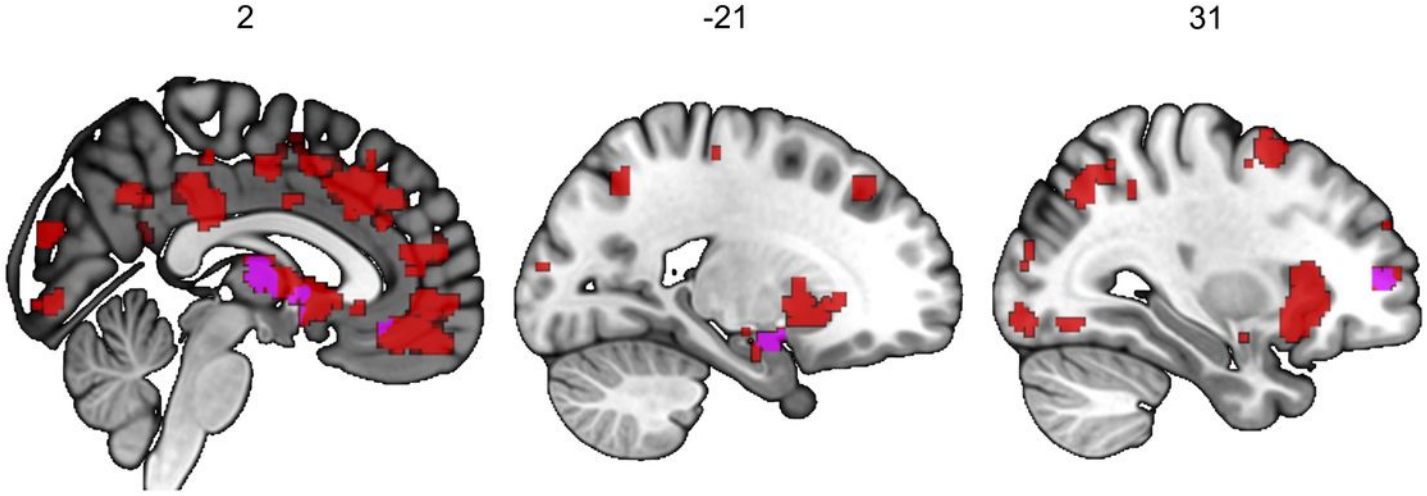
2
-21
31

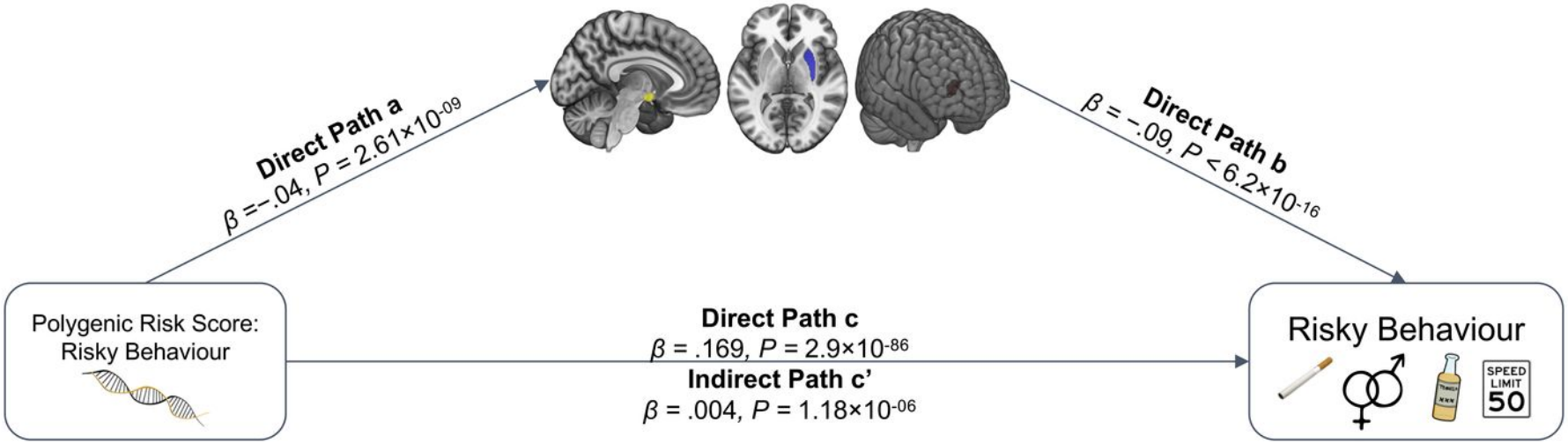
Direct Path a
β =−.04, P = 2.61×10-09
Direct Path b
β = −.09, P < 6.2×10-16
Polygenic Risk Score:
Risky Behaviour
Direct Path c
β = .169, P = 2.9×10-86
Indirect Path c'
β = .004, P = 1.18×10-06
Risky Behaviour
SPEED
LIMIT
50